Large amplitude inversion tunneling motion in ammonia, methylamine, hydrazine, and secondary amines: From structure determination to coordination chemistry

Ha Vinh Lam Nguyen, Iwona Gulaczyk, Marek Kręglewski, Isabelle Kleiner

Coordination Chemistry Reviews 436 (2021) 213797

Contents lists available at ScienceDirect

Coordination Chemistry Reviews

journal homepage: www.elsevier.com/locate/ccr

Review

Large amplitude inversion tunneling motion in ammonia, methylamine, hydrazine, and secondary amines: From structure determination to coordination chemistry

Ha Vinh Lam Nguyen [a,b,*], Iwona Gulaczyk [c], Marek Kręglewski [c], Isabelle Kleiner [a]

[a] Laboratoire Interuniversitaire des Systèmes Atmosphériques (LISA), CNRS UMR 7583, Université Paris-Est Créteil, Université de Paris, Institut Pierre Simon Laplace, 61 avenue du Général de Gaulle, 94010 Créteil, France
[b] Institut Universitaire de France (IUF), 1 rue Descartes, 75231 Paris Cedex 05, France
[c] Faculty of Chemistry, Adam Mickiewicz University, ul. Uniwersytetu Poznańskiego 8, 61-614 Poznań, Poland

ARTICLE INFO

Article history:
Received 15 October 2020
Received in revised form 7 January 2021
Accepted 10 January 2021

Keywords:
Large amplitude motion
Inversion tunneling
Molecular structures
High resolution spectroscopy
Coordination complexes

ABSTRACT

Inversion tunneling in a symmetric double minimum potential is a challenging large amplitude motion problem which causes all rotational energy levels to split into a symmetric and an antisymmetric level. Not like other types of large amplitude motion such as internal rotation, inversion tunneling appears much rarer, but the fundamental knowledge gained from this motion is essential to understand the complex structures in coordination chemistry. A double minimum potential needed for inversion tunneling requires the symmetry of the frame to which the inversion object is attached to be C_s or higher, while there is no restriction on the symmetry of the frame for internal rotation. This review summarizes four most classic examples of molecules featuring inversion tunneling motion and their coordination complexes. The textbook example, ammonia, with its umbrella motion during which the nitrogen atom passes from one side of the plane formed by the three hydrogens to the other, will be presented with information on its group theoretical considerations, theoretical studies, electronic ground state spectra in the infrared range, and its coordination complexes, especially those formed with calcium and copper. In the second classic example, methylamine, CH_3NH_2, the inversion motion of the amino group $-NH_2$ is coupled with a methyl internal rotation $-CH_3$. The spectrum of methylamine can be treated using a tunneling formalism applying the G_{12} permutation-inversion symmetry group. Extensive studies on the ground state, the first and second excited torsional states ν_{15}, the inversion wagging state ν_9, and the C-N stretching band ν_8 exist along with their combinations. Pertubations and blends have made the analysis of methylamine very challenging. The third subject is on hydrazine with complex internal dynamics governed by three large amplitude motions: two $-NH_2$ tunneling motions and an internal rotation (torsion) of the two amino groups around the N-N bond. Regarding the spectrum of hydrazine, the vibrational ground state lies in the microwave region. The first, second, and third excited torsional band ν_7, symmetric wagging ν_6, and asymmetric wagging ν_{12} are found in the infrared range. Group theoretical treatment and tunneling formalism can only be used to fit sub-bands individually, while global fits still remain a difficult task. Metal complexes with hydrazine and methylamine are introduced, proving the importance of spectroscopic understanding of molecular structures for the knowledge of coordination chemistry. Finally, secondary amines feature inversion tunneling of the hydrogen atom attached to the nitrogen, which is accompanied by two methyl internal rotations but not coupled with them so that they can be treated separately. For this class of molecules, only spectra of the vibrational ground state in the microwave domain will be considered.

* Corresponding author at: Laboratoire Interuniversitaire des Systèmes Atmosphériques (LISA), CNRS UMR 7583, Université Paris-Est Créteil, Université de Paris, Institut Pierre Simon Laplace, 61 avenue du Général de Gaulle, 94010 Créteil, France; Institut Universitaire de France (IUF), 1 rue Descartes, 75231 Paris Cedex 05, France.
E-mail address: lam.nguyen@lisa.ipsl.fr (H.V.L. Nguyen).

https://doi.org/10.1016/j.ccr.2021.213797
0010-8545/

Contents

1. Introduction

The current century has seen an extraordinary development both in theoretical and experimental approach to determine the structures of molecules, but molecular structure determination has a long tradition starting more than 100 years ago. The award of several Nobel Prizes in physics and chemistry emphasizes the importance of understanding molecular structures. Three years after the first Nobel Prize in physics was awarded to Röntgen for the discovery of X-rays, von Laue demonstrated the diffraction of X-ray in crystals [1,2]. These two scientists have laid the ground stone for an uncountable number of investigations on structures of molecules in solid state [3–11]. Among them is Bragg's study to determine the atomic arrangements of simple crystals such as ZnS, CaF_2, $CaCO_3$, and FeS_2 [12,13] which has been distinguished by the Royal Swedish Academy of Sciences in 1915, or the investigation of Debye in 1936 which contributes to human knowledge of molecular structure through the molecular dipole moments [14]. Moving to larger, chemical or biological molecular systems, the discovery of the double helix molecular structure of nucleic acids by Crick, Watson, and Wilkins received extraordinary attention in 1962 [15]. In the same year, Kendrew and Perutz revealed the structures of hemoglobin and myoglobin [16–18]. Two years later, Hodgkin determined structures of important biomolecules like B_{12} and penicillin [19,20]. Many spectroscopic methods have been developed to unveil the structures of molecules in different states of aggregates, employing the whole electromagnetic range and offering even higher resolution and accuracy. Only to mention some of them, and not exhaustively, are X-ray crystallography, electron microscopy, neutron scattering, nuclear magnetic resonance, infrared, microwave, terahertz, and ultraviolet–visible spectroscopy. Their development and interplay have addressed increasingly challenging questions in the past, and understanding more complex molecular structures using spectroscopy will remain an important aspect in the future.

Determining the structures of even small molecules, however, can become a very challenging task if intramolecular dynamics occur, causing energy levels to split into several levels due to tunneling effects [21]. Two representatives of large amplitude motions (LAMs) are internal rotation, typically of a methyl group involving a three-fold potential, and inversion tunneling upon a two-fold potential. Internal rotation has been extensively studied along the development of rotational spectroscopy with many investigations on complex problems such as low torsional barrier and coupled internal rotors [22–26]. The inversion motion is demonstrated well in ammonia, NH_3, where it concerns the tunneling of the nitrogen atom through a plane which is spanned by three hydrogen atoms [27]. This "umbrella" motion connects two energetically equivalent forms of ammonia, causing splittings of all rotational transitions of a certain symmetry, from which the tunneling barrier height can be deduced. Inversion tunneling does not only occur in ammonia, but also in larger molecules like ethylene diamine [28] hydrazine [29] phenyl formate [30] phenol [31] *gauche*-1,3-butadiene [32] some dimers [33,34] and especially complexes [35–38].

Weakly bounded complexes were studied in the gas phase extensively by rotational spectroscopy since the technique of molecular jet Fourier transform microwave spectroscopy exists [39]. Among them, complexes involving the ammonia sub-unit form an important subject. Because of the strong capabilities for binding hydrogen bonds, ammonia has similar solvation capacities as water. Concerning the coordination chemistry of metal ions in solution, obtaining detailed information about solute–solvent interactions has never been straightforward. A number of experimental techniques have been developed towards that goal, such as X-ray diffraction, which can determine the structures as aforementioned. Knowledge on interactions between a metal atom and ammonia can be also achieved by studying small complexes in the gas phase as well as through information about the structures of solvated metal ions for which spectroscopy is an essential

tool. In the visible or ultraviolet spectral range, alkaline-earth metals solvated by molecules were studied using electronic spectroscopy combining molecular beams and mass-selected laser photodissociation [40–42]. Infrared photodissociation spectroscopy was also used to study solvated alkali-metal ions [43,44]. The inversion of pyramidal and tetrahedral molecules AX_3 and AX_4 including complexes with metal has been reviewed by Boldyrev and Charkin [45]. Organometallic intramolecular-coordination compounds containing a nitrogen donor ligand are also studied [46].

Tunneling motions also occur in methylamine, a molecule which plays a significant role in coordination chemistry. With a lone pair of electrons on the nitrogen atom, methylamine can coordinate with metal ions to create various types of complexes [47,48]. Some of the complexes are widely used in supramolecular chemistry as polymeric networks [49]. A variety of networks can be achieved on the basis of multidentate flexible ligands, which are able to take up different interesting conformations like boxes or helices depending on the properties of the metal ions. Exemplary compounds having such abilities are silver (I) salts with flexible multidentate ligands based on pyridylmethylamine. A lot of interest was focused on clusters of alkali metal atoms with the ammonia derivative methylamine as solvating agent [50]. A number of studies were performed to describe the change of ammonia into methylamine on the alkali cation and solvated electrons, i.e. those on the infrared spectra of $Li(NH_2CH_3)_{3-5}$ [51]. The coordination chemistry of methylamine also plays an important role in medicine. For example, anticancer activity and solubility of *cis*-platin can be improved by methylglycine and methylamine ligands against human breast cancer [52].

Hydrazine, $NH_2{-}NH_2$, features two amino groups undergoing three LAMs. They are the two inversion motions, one for each amino group, and the internal rotation about the N–N bond. The rotational spectrum of hydrazine had been first assigned by Kasuya et al. [29] and the investigation was then improved by Tsunekawa, Kojima, and Hougen [53]. As a coordination complex partner, the *gauche* conformation of hydrazine, where one amino group is twisted from the *trans* or *cis* positions, comes into play. In sp^3 hybridization, the two lone electron pairs occupy the vacant tetrahedral positions. Being the source of the nucleophilic and basic character of the molecule, the lone pairs are able to coordinate to a metal ion in two ways as a ligand, either monodentate or bridged bidentate. Metal hydrazine complexes can include different anions such as perchlorate, oxalate, azide, nitrate, carboxylate, and sulfate [54]. In most of these complexes, hydrazine appears as a bridged bidentate ligand. The chemistry of hydrazine and its derivatives including many different types of complexes involves a large number of scientific works, for example on its inorganic derivates, metal hydrazines, hydrazine salts, hydrazinium metal complexes, and metal hydrazine carboxylates. Transition metal complexes with monodentate and bridging hydrazines are very popular. A lot of hydrazine complexes with a number of metals and anions have been synthesized, and their structures been characterized by different methods [55,56]. Metal ions forming complexes with hydrazine are often silver, calcium, copper, cobalt, chrome, iron, mercury etc. with anions like carbonate, halide, and nitrate [57].

While inversion motions involving nitrogen are interesting physical phenomena by themselves, in most relevant ligand forms of ammonia, methylamine, and hydrazine, the inversion motion is quenched, at least to accuracy of the metal–ligand experiments. Conformational strain and structural rigidity can effectively prevent the inversion of amino groups by increasing the inversion barrier. Another way to quench the inversion is to form a nitrogen stable chirality center by coordination of the electron lone pair of nitrogen to a metal center [58]. Knowledge on factors that can increase or decrease the inversion barrier allows us to control molecular motions. For example, the pyramidal inversion of nitrogen in aziridine molecules is blocked by metal complexation and the decomplexation restores the fast inversion in "switch-type" molecular process [59]. Recently, the importance of quantum chemical inversion effects of nitrogen was demonstrated in a human dipeptidyl-peptidase containing zinc that hydrolyses dipeptides [60]. This study presents the first modeling of the reaction mechanism for this peptidase. Water addition on amide carbon atoms and nitrogen inversion, i.e. change of pyramidalization on the leaving nitrogen when the amino group goes from the planar sp^2 to the pyramidal sp^3 configuration, is shown to be the rate-determining steps. The nitrogen inversion occurs in a concerted way followed by a hydrogen bonding with a glutamine amino acid, immediately "blocking" the system into the configuration where reversion to the enzyme–substrate complex is not possible.

Looking back at the history of rotational spectroscopy over a century, there are considerably fewer investigations on inversion tunneling compared to the vast number of studies on the other type of LAM, internal rotation. The main reason is that for internal rotation, there is no restriction on the symmetry of the frame, while a double minimum potential requires the symmetry of the frame to which the inversion object is attached to be C_s or higher. Moreover, if the molecular structure allows for it, inversion tunneling is very often accompanied by internal rotation. A typical example is the proton inversion in primary amines which is always combined with the internal rotation of the amino group [53,61–63]. Regarding complexes, symmetry breaking by complexation often quenches inversion motions, as for example in tropolone, a seven-membered aromatic ring, in which proton tunneling occurs [64–67]. Doublet splitting appears in electronic spectra and the potential energy surface has two minima [68]. Once tropolone is bound to other molecules, the double minimum disappears. In tropolone complexes with water and methanol, the fluorescence excitation spectra do not reveal any doublet splittings, showing that the proton tunneling is effectively quenched [69–72]. This supports the assumption that by intermolecular hydrogen bond formation, the inversion coordinate becomes so asymmetric that no tunneling doublet is observed.

The present review will give an overview on the large amplitude tunneling motions of four most important representatives: (i) Ammonia with a pure tunneling motion of the nitrogen atom; (ii) Methylamine where the inversion motion of the amino group $-\mathbf{NH_2}$ is coupled with a methyl internal rotation $\mathbf{-CH_3}$; (iii) Hydrazine with complex couplings between two $-\mathbf{NH_2}$ tunneling motions and $-\mathbf{NH_2}$ internal rotations; and (iv) Secondary amines where the $-\mathbf{NH}$ proton inversion tunneling is accompanied by two methyl internal rotations but not coupled with them. For each molecule, applications of structure determinations from spectroscopy to understand coordination chemistry are introduced.

2. Ammonia

In coordination chemistry, ammonia (NH_3) plays an important role: it is a ligand within the so-called metal "ammine" complexes where ammonia is bound to metal ions. Information on the isolated molecule allows us to study the intrinsic properties of ammonia to understand its role in complexes, and therefore will be focused on first.

Global ammonia emissions have at least doubled since the pre-industrial period mainly due to the intensification of agriculture and the use of fertilizers. Although ammonia is a species with a lifetime of only a few hours in the Earth's atmosphere, it is nevertheless a dreadful pollutant which accelerates the formation of particles, and a precursor of secondary aerosols which reduce air quality. It represents therefore a very strong climatological concern

today. Unknown source, due to intense farming and industry, of ammonia have recently been detected by the Infrared Atmospheric Sounding Interferometer (IASI) on board of the METOP satellite [73,74].

In addition to its relevance to the Earth's atmosphere, ammonia is also a very important species to understand the physical properties of gas giant planets [75] and cool brown dwarfs [76,77]. It is the fourth abundant compound in the atmosphere of the planet Jupiter. Although not yet been detected, scientists also expect its presence in exoplanets [78]. Meaningful interpretation of any atmospheric spectra relies on accurate knowledge of spectroscopic parameters of even minor abundant gases involved, and in particular ammonia.

Ammonia also attracted academic attention for its spectroscopy challenge arising from the large amplitude inversion tunneling motion. This is the above-mentioned "umbrella motion" during which the nitrogen atom tunnels from one side of the plane formed by the three hydrogen atoms to the other [27]. These two configurations are separated by a potential barrier with a height on the order of 2023 cm^{-1} (see Fig. 1). The tunnel effect separates the doubly degenerated inversion energy levels into a pair of levels called the symmetric, "*s*", and antisymmetric, "*a*", levels, sometimes called the inversion +/– levels [21]. Often used as a model molecule, ammonia has been the subject of intensive spectroscopic works. In the present review, we focus on the electronic ground state of its gas phase spectrum.

2.1. Group theoretical considerations

If the large amplitude inversion motion is neglected, it is easy to see that the pyramidal shape of NH_3 belongs to the C_{3v} symmetry group, containing a C_3 axis (see Fig. 2). If the molecule is rotated around that axis by an angle of 120° or 240°, we obtain two configurations equivalent to the initial configuration. The corresponding symmetry elements are C_3 and C_3^2. The other symmetry elements are three planes, called σ_v, σ_v', and σ_v'', which contain the nitrogen atom and one of the three hydrogen atoms.

If we now consider the tunneling motion between the two equivalent equilibrium configurations of NH_3 (see Fig. 1), the C_{3v} group is no longer suitable to describe this molecule, as it does not contain any symmetry element allowing to switch from one configuration to the other. This motion requires an operator for the reflection through a plane perpendicular to the C_3 axis, as shown in Fig. 3. To treat properly the inversion motion, Bunker and Jensen used an extended permutation-inversion group, G_{12}, which is isomorphic to the molecular symetry group D_{3h} [79]. The character table and irreducible representations of this group can be found in Ref. [79]. Ammonia can also be described in a so-called "reference configuration" depending on the inversion coordinate γ shown in Fig. 1. Each internal motion of the molecule, such as vibration, rotation, and inversion, will be described following the irreducible representations A_1', A_2', A_1'', A_2'', E', and E'' of the D_{3h} group.

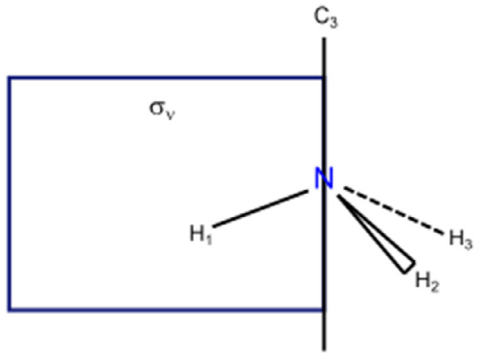

Fig. 2. The operators of NH_3 in the C_{3v} group.

2.2. Quick overview of the infrared spectroscopic studies

The spectroscopy studies on ammonia can be devided into two sections dealing with (i) the experimental spectral dataset fitted using effective Hamiltonians and (ii) theoretical studies of the spectrum of ammonia using quantum chemical calculations which also sometimes combine experimental and theoretical results.

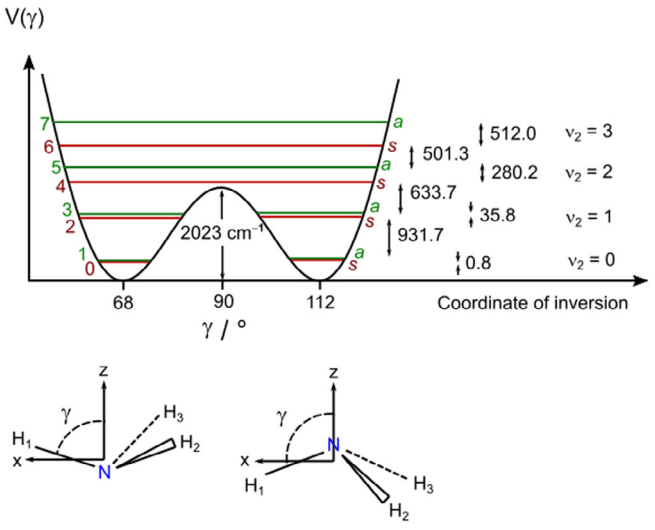

Fig. 1. Upper trace: The two-fold potential of NH_3 along the inversion coordinate γ, showing the inversion vibration mode ν_2 and the first excited energy levels labeled ν_2 = 1, 2, and 3. Each sub-component is either labeled *a* or *s* (right hand side of the potential curve). An alternative labling of the energy levels uses a ν_{inv} quantum number (left hand side). Lower trace: the two equivalent equilibrium configurations of NH_3.

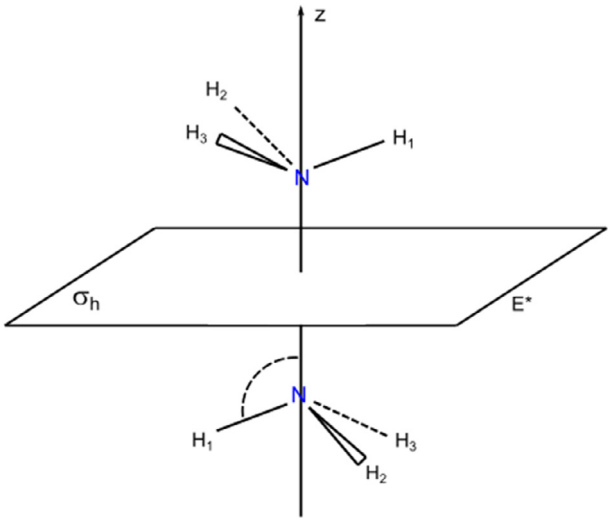

Fig. 3. The two equivalent equilibrium configurations of NH_3, with the plane σ_h perpendicular to the C_3 axis (the z axis). This operator corresponds to the E* operation in the G_{12} permutation-inversion group of NH_3, isomophic to the symmetry group D_{3h}.

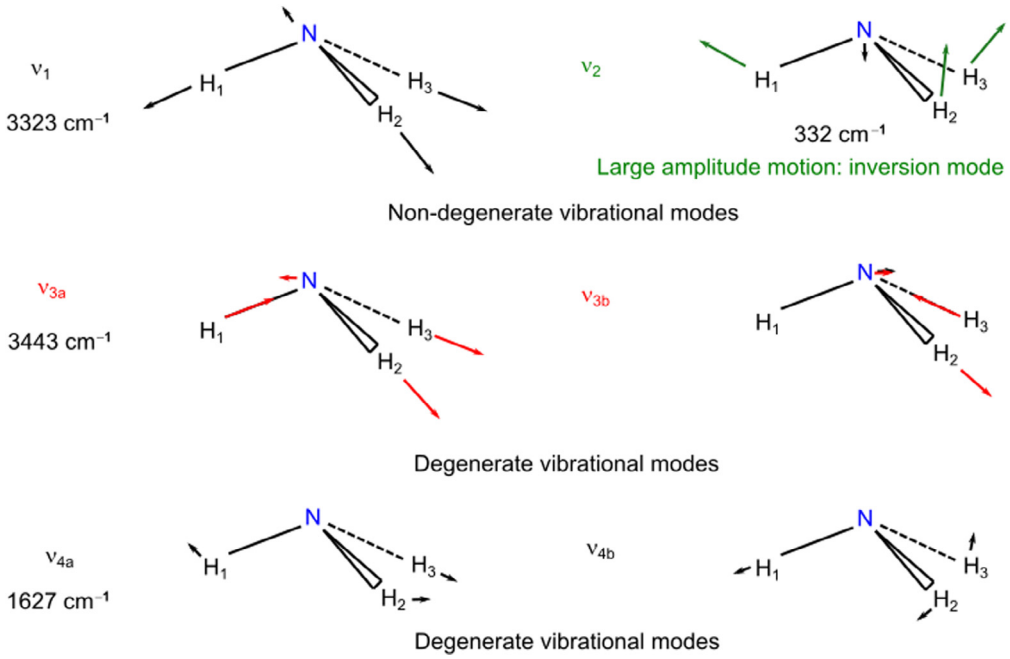

Fig. 4. The vibrational modes of ammonia. For the degenerate modes, two orthogonal components are depicted.

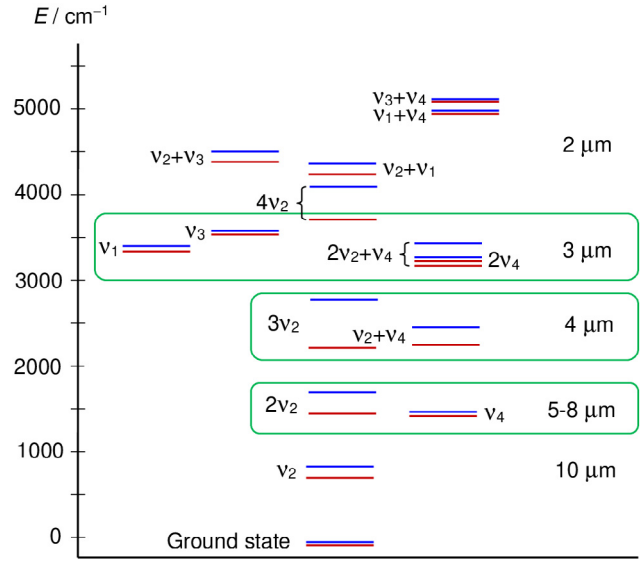

Fig. 5. Vibration-inversion energy levels of NH_3 up to 5000 cm^{-1}. On the right hand-side, the infrared spectral range corresponding to the transitions from the fundamental state is given. The circled regions illustrate the various polyads (see text). Red energy levels are the symmetric states, and blue ones are the asymmetric states.

2.2.1. Vibration-inversion-rotational Hamiltonian and fits of experimental data

In the harmonic normal mode approach, apart from the inversion mode (ν_2) of the LAM, NH_3 has another non-degenerate (one-dimensional) mode, the ν_1 stretching mode, and two degenerate (two-dimensional) bending modes, ν_3 and ν_4, as shown in Fig. 4. The degenerate modes correspond to two components labeled ν_{3a} and ν_{3b} or ν_{4a} and ν_{4b} in Fig. 4, vibrating at the same frequencies. They also require an additional quantum number, the vibrational angular momentum ℓ. The various components of a given degenerated mode can interact with each other, introducing the so-called "ℓ-type terms" of the Hamiltonian.

To model the excited vibration-inversion-rotational states, the treatment is to divide the vibration-inversion energy levels of NH_3 into small "polyads", as illustrated in Fig. 5. The polyads are sets of energy levels which interact with each other. The challenge is the existence of a strong coupling between the large amplitude inversion motion in NH_3 and other small amplitude vibrations. The higher in energy, the more complex the situation. However, the couplings between levels belonging to different polyads can be neglected after having been previously made negligible by appropriate contact transformations of the Hamiltonian of the system. Such an approach was proven to be very satisfactory and led to excellent results, in particular in the regions of 4 μm [80] 3 μm [81,82] 5–8 μm [83–85] and 10 μm [86–90].

The room temperature spectrum of ammonia is implemented in the HIgh resolution TRANsmission molecular absorption database (HITRAN) [91] with over 29 000 experimental transition frequencies and intensities for its two isotopologues $^{14}NH_3$ and $^{15}NH_3$. A complete description of the HITRAN database latest updates for NH_3 is given by Down et al. [92].

2.2.1.1. The 10 μm window. The energy parameterization of NH_3 was developed a long time ago, first by Spirko et al. [93] and followed by Urban [94]. Later, Pracna et al. [95] performed a similar parameterization of the intensities. Papoušek et al. [96] introduced the idea to choose a reference configuration following the large amplitude inversion motion in such a way that all other small amplitude vibrations remain small. Their pioneer work allowed for a vast set of follow-up studies until today. Used in atmospheric detection, many studies were dedicated to very high accuracies of the line intensities and line widths for the ν_2 band [86–90].

2.2.1.2. The 5–8 μm and the 4 μm windows. In the 5–8 μm window, absorption is mainly due to the $2\nu_2$ and the ν_4 fundamental bands. The former corresponds to the first overtone of the inversion or umbrella motion, and the later to a doubly degenerate mode. A pioneer work on the assignment of ammonia spectra is that of Benedict in 1958 [97]. The experimental measurements and data analysis have been extensively extended by Cottaz et al. [83] and Pearson et al. [85]. They combined the microwave frequencies

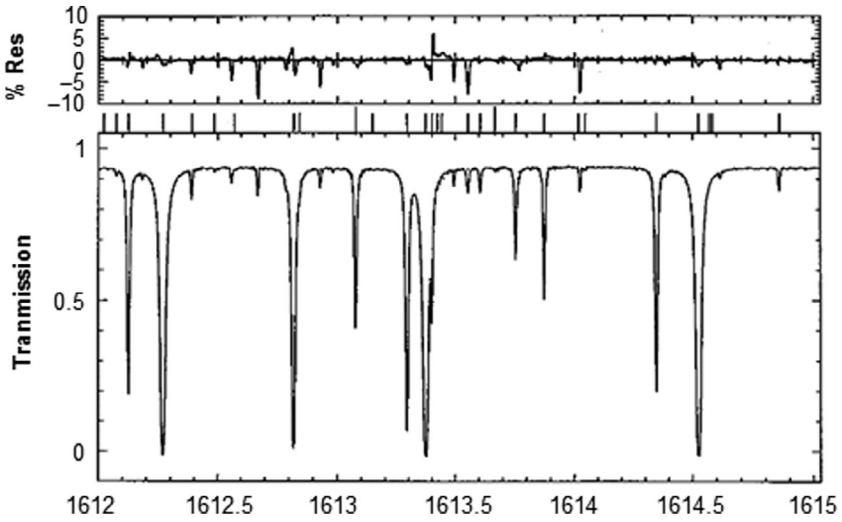

Fig. 6. Comparison of calculated and observed spectra of ammonia in the $2\nu_2/\nu_4$ bands. The lower panel shows the observed spectrum taken at 0.0056 cm^{-1} resolution and room temperature (pressure: 5.5 Torr and path: 0.25 m). The upper panel shows the observed-minus-calculated values in % of the residuals. The lines belonging to the hot band $\nu_{2+}\nu_4$-ν_2 located at 1612.56, 1612.67, 1612.93, 1613.49, and 1614.02 cm^{-1} are well-reproduced [84].

and the high resolution infrared spectrum recorded using the synchrotron SOLEIL (Saint-Aubin, France) and achieved a fit within experimental microwave and infrared accuracy. This spectral region is particularly interesting not only for probing the atmosphere at depth, but also from a fundamental point of view. Although the investigated energy level system is relatively simple concerning the $2\nu_2/\nu_4$ dyad with two excited states ν_2 = 2 and ν_4 = 1 interaction, it is nevertheless an "intermediate" energy region close to the top of the potential barrier hindering the inversion, where it is always challenging but interesting to test theoretical models. The two excited states interact through a vibration–rotation Coriolis coupling type, if they are connected by terms in the kinetic part of the Hamiltonian, or a Fermi-type if they are connected through the potential part.

In the 4 μm window, we found the interacting $3\nu_2/\nu_2 + \nu_4$ dyad [80]. Beside the fundamental bands, the 4–8 μm spectral range contains a number of hot bands coming from excited states populated at room temperature, i.e $3\nu_2$-ν_2, $\nu_2 + \nu_4$-ν_2 (in the 5–8 μm range), $4\nu_2$-ν_2, ν_1-ν_2, ν_3-ν_2, and $2\nu_4$-ν_2 (in the 4 μm range) [84] which are important to reproduce correctly the infrared spectra. Fig. 6 illustrates a portion of the spectrum with the observed and calculated % of the residuals in the upper panel, showing that the lines belonging to the hot band $\nu_2 + \nu_4$-ν_2 located at 1612.56, 1612.67, 1612.93, 1613.49, and 1614.02 cm^{-1} are well-reproduced.

2.2.1.3. The 3 μm window. In this spectral window, at least three bands interact (see Fig. 5). The fundamental bands ν_1 and ν_3 whose *s* and *a* components for the former are located at 3336.107 and 3337.095 cm^{-1}, respectively, and for the latter at 3443.627 and 3443.988 cm^{-1}. For the first harmonic $2\nu_4$ band, the *s* component is located at 3216.103 cm^{-1} and the *a* component at 3217.783 cm^{-1} for the non-degenerate state and at 3240.441 and 3241.621 cm^{-1}, respectively, for the degenerate state. Kleiner et al. [81] performed a prediction of the frequencies and intensities of all NH_3 transitions with values of the rotational quantum number *J* up to 10 and an intensity greater than 10^{-6} cm^{-2}·atm^{-1}. This limit was sufficient for the analysis of planetary spectra.

2.2.2. Theoretical studies

The effective Hamiltonian polyad approach shows some limitations above 3 μm, i.e. from 4791 to 5294 cm^{-1}, where the number of interacting states increase and empirical line parameters are available [98]. The most probable energy of the lower state of unassigned transitions can be performed using the temperature dependence of the intensity ratio between unassigned and already assigned transitions, as done in the 6626–6805 cm^{-1} range [99]. Theoretical studies can help to improve this issue [100–103]. Down et al. combined empirical energy levels with calculated intensities, leading to a final list of more than 40 220 lines [92] by using the variational line list calculated by Yurchenko, Barber, and Tennyson [102]. These calculations are based on an empirically refined potential energy surface [103] *ab initio* dipole moment surface [104] and the program suite called TROVE [105] working with a unique local mode representation. All resonances between vibrational states are taken into account. Combining experimental frequencies with dipole moments obtained from *ab initio* is known to produce very reliable transition intensities [103–107].

2.3. Ammonia complexes

Complexes involving ammonia as sub-unit were the subject of a number of papers. The structure of ammonia-water, for example, was determined by Herbine and Dyke [108]. The microwave (from 36 to 86 GHz) and far infrared (from 520 to 800 GHz) spectra of this dimer were then investigated by Stockman et al. in 1992 [109]. The ammonia moiety can internally rotate around its C_{3v} axis, while the water subunit can tunnel or invert between two equivalent configurations in a two-fold potential barrier, and these two LAMs interact. The ammonia internal rotation splits the states into the A species, corresponding to one of the ammonia proton spin functions, I = 3/2, and the E species, corresponding to the I = 1/2 spin function. Stockman et al. found two sets of splittings in the spectrum [109]. One of them (around 10 GHz) corresponds to the internal rotation of ammonia and the very low barrier hindering this torsion was determined to be around V_3 = 10.5 cm^{-1} using the observed splittings. The second set of splittings (around 113 MHz) which is illustrated in Fig. 7 was attributed to arise from the water tunneling with an estimated barrier of around 800 cm^{-1} [109].

The ammonia-benzene dimer was studied by Rodham et al. [111]. The experimental and *ab initio* results predict that the ammonia monomer can (almost) freely rotates internally above the benzene plane. The three hydrogen atoms of ammonia interact with the π electrons of the benzene ring. The smaller dissociation

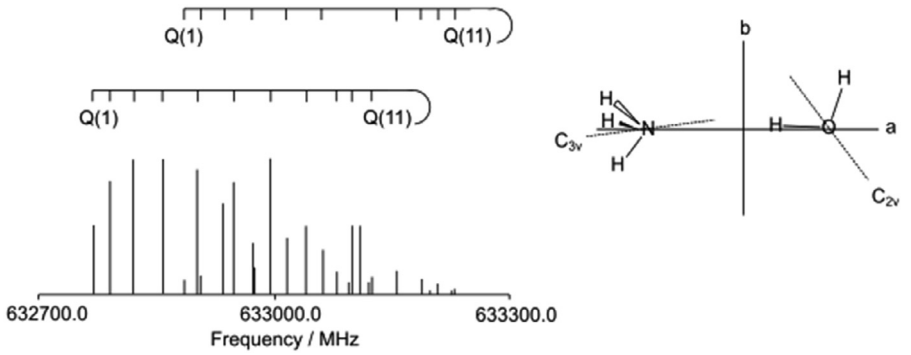

Fig. 7. Left hand side: A section of the far infrared spectrum observed by Stockman et al. [109] Above the spectrum, the assignments for two series of lines belonging to a *Q*(*J*)-branch, where the rotational quantum number *J* does not change during the transition ($\Delta J = J' - J'' = 0$) from $J = 1$ to $J = 11$, are given. The two series of assignments correspond to splittings due to the water inversion. Right hand side: the equilibrium structure of ammonia-water in the principal axis system calculated by Latajka and Scheiner [110] and the symmetry axis of each monomer.

energy corresponds to a weak hydrogen donor character of ammonia. It is quite interesting to note that benzene-ammonia is a rare example of ammonia being a proton donor in weakly bound complexes. Ammonia can also form complexes with HCCH [112] and HCF_3 [113] or with rare gas as reported in the study on ammonia-argon by Nelson et al. [114] It was shown in the latter paper that the ammonia subunit inverts within the complex and van der Waals interactions affect the ammonia large amplitude inversion and tunneling motion. Methanol-ammonia, CH_3OH-NH_3 and $^{13}CH_3OH$-NH_3, complexes were studied by Fraser et al. in 1988 [115]. The microwave spectrum reveals interesting and complicated splitting patterns arising from both the internal rotation of the methyl group in methanol and of the ammonia moiety. The authors concluded that the structure of the methanol-ammonia complex is similar to that of water-ammonia, i.e. an almost linear complex where the hydrogen bond is collinear with the symmetry axis of NH_3 (see Fig. 7) [115]. Last but not least, let us mention the recent work of Surin et al. where for the first time the gas phase rotational spectrum of the van der Waals complex NH_3-H_2 has been observed [116].

In the condensed phase, amines are considered as amphoteric as they can act both as a donor and acceptor of protons in hydrogen bonds. Concerning the coordination chemistry of metal ions in solution, obtaining detailed information about solute–solvent interactions is a challenging task. To learn more about the interactions between a metal and ammonia, it is important to study small complexes where spectroscopy can be useful to get information about the structures of solvated metal ions. In the ultraviolet–visible spectral range, alkaline-earth metals solvated by molecules were investigated by electronic spectroscopy combining molecular beams and mass-selected laser photodissociation [40–42]. Solvated alkali-metal ions were also studied by infrared photodissociation spectroscopy [43,44].

Recently in 2018, the gas phase infrared spectra of $Ca(NH_3)_n$ complexes, formed by laser ablation in presence of a molecular beam with ammonia, have been recorded [117] revealing a structure with the ammonia molecules around a central calcium atom. In 2009, combining laser ablation of a metal and co-expansion with a mixture of argon and ammonia gas, Ohashi et al. were able to produce ammonia solvated metal ions $M^+(NH_3)_n$ where M = Ag and Cu [118]. Using infrared spectroscopy to study the coordination chemistry of ammonia with metal ions combined with density functional theory, the authors succeeded to determine the structure of the shells formed by the ammonia molecules surrounding the ions (see Fig. 8). The infrared spectra obtained for $Cu(NH_3)_3$ and $Cu(NH_3)_4$ are very different. In the $Cu(NH_3)_4$ complex, the presence of a NH···N hydrogen bonding produces new absorption bands in the spectrum, demonstrating the importance of using infrared spectroscopy to explore the structure of coordination complexes.

The coordination of ammonia with silver ions was also studied by the same authors using infrared photodissociation spectroscopy [119]. They found that for $Ag(NH_3)_3$ or $Ag(NH_3)_4$ the infrared spectrum shows absorption signatures near the frequencies of the isolated ammonia, which tends to demonstrate that each ammonia molecule is individually coordinated to Ag^+. The same technique was used by Imamura et al. to study coordination chemistry with cobalt and nickel [120]. Finally, in 2019 a study combining photofragment spectroscopy with calculations at high level of theory produced an assignment for the vibrational spectra of $Cr^+(NH_3)_{1-6}$ in the N-H stretching region (2950–3600 cm^{-1}) [121].

3. Methylamine

Methylamine, CH_3NH_2, is an organic molecule containing seven atoms and the simplest primary amine in chemistry. It is a precursor of glycine, the simplest amino acid. Some experimental studies have presented reaction pathways for the formation of glycine in water with ice which starts from methylamine and carbon dioxide exposed to high energy electrons [122] or ultraviolet radiation

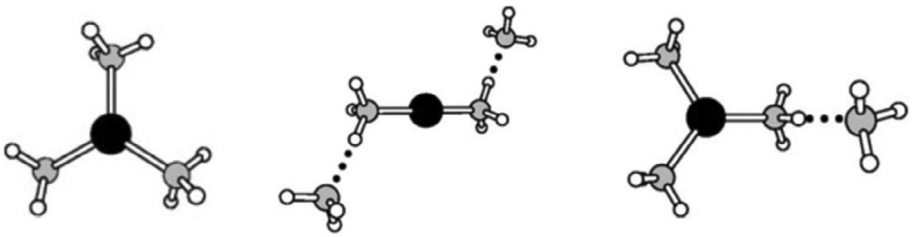

Fig. 8. Left hand side: The coordination complex structure of $Cu^+(NH_3)_3$. Middle and right hand side: two conformers structures of $Cu^+(NH3)_4$. The structures are calculated by Ohashi et al. using the DFT method [118].

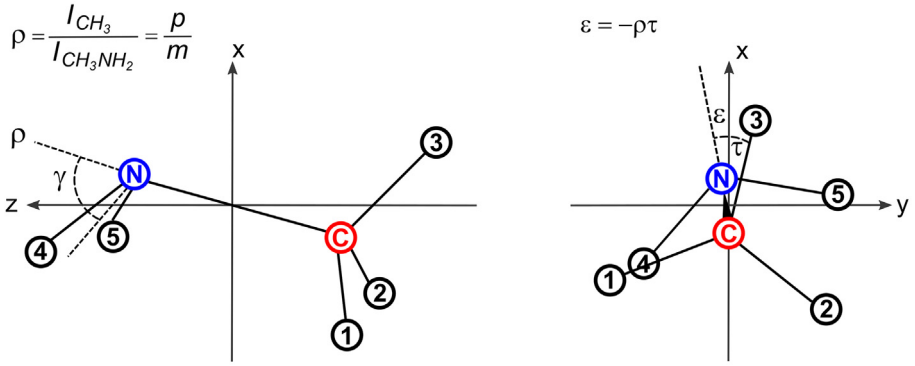

Fig. 9. A schematic view of a methylamine molecule presenting two large vibrational coordinates, an inversion coordinate γ and a torsional coordinate τ. The calculation of ρ is given in the left hand side equation, where p and m are integer. The angle ε changes with the torsional angle τ to minimize the inversion-rotation coupling.

[123,124]. In similar conditions, glycine can be decomposed producing CH_3NH_2 and CO_2 [125]. Methylamine together with other methyl-substituted amines like dimethylamine, $(CH_3)_2NH$, and trimethylamine, $(CH_3)_3N$, plays an important role in various biological processes and organic syntheses. They are also considered as efficient corrosion inhibitors of aluminum. Methylamine has been detected in the interstellar medium for the first time toward Sgr B2 in 1974 at 3.5 cm [126] and at 3 cm [127]. In 2011 it was observed in a spiral galaxy situated in front of quasar PKS 1830-211 with a redshift of 0.89 [128]. Methylamine among other amines and amino acids was also detected in cometary samples of the Stardust mission [129}. Recently, methylamine was identified in three hot cores in the high-mass star forming region NGC 6334I [130]. Like ammonia and other molecules having a free pair of electrons, methylamine and its derivatives play a significant role in coordination chemistry as ligands.

3.1. Internal dynamics of methylamine

Beyond the technological and astrophysical importance of methylamine, this molecule is very interesting from its rich structural features involving large amplitude vibrations. It is a non-rigid (floppy) molecule performing two different types of LAMs: the hindered torsion of the methyl group $-CH_3$ about the C-N bond (ν_{15} torsional motion) and the internal inversion of the amino group $-NH_2$ (ν_9 wagging motion). Although methylamine is a very simple molecule from chemical point of view, it has been of great interest for spectroscopists over decades. Its internal dynamics are strongly determined by these two coupled LAMs, which give rise to a rotation-inversion-torsional structure in the vibrational states. It is well-known that the use of linear coordinates to describe large amplitude vibrations is inappropriate. No single linear coordinate can correctly describe the large changes in molecular configurations, such as internal rotation or inversion, without describing large changes in the values of other linear coordinates. On the other hand, it is much easier to build the quantum–mechanical operators in linear coordinates, because then the tensor matrix elements are not functions of these coordinates [131] which is not correct when curvilinear coordinates are used. Therefore, the number of curvilinear coordinates describing the large amplitude vibrations should be minimized, whereas other vibrations should be described by the linear coordinates.

In methylamine, the inversion and internal rotation motions need to be described with the minimum number chosen for curvilinear coordinates being two. The inversion coordinate γ is defined as the angle between the HNH bisector and the C-N bond. The torsional coordinate τ is the angle between the NCH plane and the plane of symmetry of the NH_2 group. Both large amplitude coordinates are presented in Fig. 9. To minimize the rotation-inversion coupling, the angle ε changes with the inversion angle γ. With ρ being small, the amino group is fixed to the molecular axis system, leading to a strong coupling between rotation and torsion.

The barriers of 23.2 kJ·mol^{-1} and 8.6 kJ·mol^{-1} in the potential functions of methylamine for the inversion and the torsion, respectively [62,132] are not very high and the LAMs are coupled strongly with the overall rotation of the molecule. Therefore, the structure of rovibrational energy levels of methylamine is affected by the tunneling splittings. Even in the ground state, energy splittings are observed, meaning that the methylamine high resolution spectra are extremely difficult to analyze and require a special theoretical approach. Not only for methylamine, but also for many other non-rigid molecules, the Hamiltonian has to be adapted or even individually developed to fit the molecular spectra.

3.2. The tunneling formalism

In 1987, Hougen and Ohashi [133] developed a theoretical formalism to fit rotational energy levels in isolated vibrational states of methylamine. The formalism assumed that both LAMs can be treated in the high-barrier limit. The torsional-wagging part of this approach was derived separately from the torsional-wagging-rotational part. The most important steps for setting up a tunneling Hamiltonian can be summarized as follows. Firstly, all conformations of the minimum energy, called equivalent equilibrium frameworks, should be found for a given molecule. To each of them, the appropriate set of rotation-vibration wave functions of small vibration coordinates and energy levels should be attached. Secondly, all feasible tunneling paths between each pair of frameworks should be found. Group theory is used to determine the number of independent tunneling parameters. Finally, following these steps, a Hamiltonian can be set up and diagonalized.

The amino group in methylamine performs a back and forth motion which induces a 60° corrective internal rotation of the methyl group, giving rise to six frameworks. Fig. 10 presents the equilibrium frameworks for methylamine. The six minima are connected by two kinds of tunneling paths. If we consider the tunneling motion from framework 1 to 3, it is clear that in this tunneling only internal rotation takes place, since the torsional angle τ changes by 120°. No inversion is involved in the motion, which can be recognized by the fact that the inversion coordinate γ does not change. If the tunneling motion from position 1 to 2 is considered, both types of tunneling are involved, since the torsional angle changes by 60° and the inversion coordinate changes its sign from positive to negative. Because of the back and forth motion of the methyl group, the scheme of six conformations is repeated *m* times to reduce the rotation-torsion coupling in the molecule-fixed axis

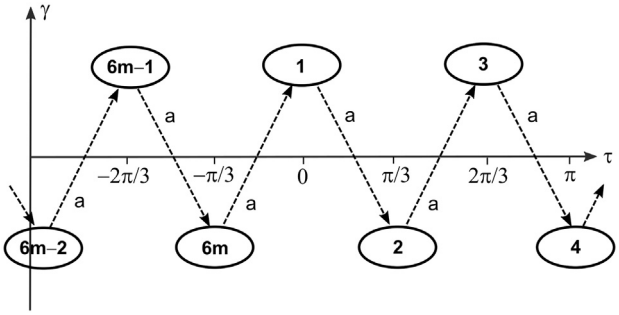

Fig. 10. A schematic representation of equivalent equilibrium frameworks (minima) on a two-dimensional potential surface for methylamine.

system. This is accomplished by a counter rotation of the molecular axis system by $-\rho\tau$ when rotating the methyl rotor by $+\tau$. In the tunneling formalism, we assume that in one minimum, a complete set of vibration–rotation states is placed and it will interact with a set of such states in a neighboring minimum.

Since methylamine is not rigid, its symmetry has to be described by the permutation-inversion group theory, not by its point group. Thus, its permutation-inversion group and extended group are extensively applied to determine the allowed terms in an effective rotational-tunneling Hamilton operator. Methylamine belongs to the point group symmetry C_s if considering only its rigid equilibrium geometry and, with inclusion of LAMs, to the G_{12} permutation-inversion symmetry group (in fact it is the m-fold extended group G_{12}^m). The G_{12} symmetry group is the Longuet-Higgins group [134] of the permutation and permutation-inversion operators E, (123)(45), (132)(45), (123), (132), (45), (23)(45)*, (12)(45)*, (13)(45)*, (23)*, (12)*, (13)* of identical atomic nuclei. The three hydrogen atoms of the methyl group are numbered 1, 2, 3 and the two of the amino group 4, 5. The G_{12} group is isomorphic to C_{6v} and there are two group operators $a \equiv (123)(45)$ and $b \equiv (23)(45)^*$ with the orders of 6 and 2, respectively. The notation (45) means a permutation of hydrogen atoms in the amino group, (123) stands for cyclic permutation of hydrogen atoms in the methyl group, and a star indicates an inversion operation in the center of mass of position of all nuclei and electrons. The character table of the group G_{12} is presented in Table 1.

The vibration–rotation wave functions are functions of small vibration coordinates, angles γ and τ, and Euler angles. Since the inversion-rotation problem is studied by the zeroth order approximation, the small amplitude vibration coordinates are set in the Hamiltonian. The effects of symmetry group operations on Euler angles χ, ϑ, φ, and on the γ and τ angles are summarized in Table 2. These effects were described by Kroto and Papoušek [135,136]. Thus, Table 2 presents the transformations of the molecular variables for an effective Hamiltonian by the permutation-inversion generators of G_{12}. The rotational variables are denoted as χ, ϑ, φ, the torsional variable as τ, and the inversion variable is γ. The group operator a rotates the methyl top by 60° and inverts the amino group. The operator b reverses the rotation of the methyl group and does not change the amino group.

The formalism proposed for methylamine by Ohashi and Hougen [133] treats each state under study as an isolated state split into sublevels with A_1, A_2, B_1, B_2, E_1, and E_2 symmetry. The effective Hamilton operator for methylamine is expressed by:

Table 1
Character table for the permutation-inversion group G_{12}.

	E	(123)(45) (132)(45)	(123) (132)	(45)	(23)(45)* (12)(45)* (13)(45)*	(12)* (13)* (23)*	
A_1	1	1	1	1	1	1	P_x, P_y, P_z[a]
A_2	1	1	1	1	−1	−1	μ_x, μ_y, μ_z[a]
B_1	1	−1	1	−1	1	−1	
B_2	1	−1	1	−1	−1	1	
E_1	2	1	−1	2	0	0	
E_2	2	−1	−1	2	0	0	

[a] Symmetry species of the laboratory-fixed components of the total angular momentum operator P and the electric dipole moment operator μ.

Table 2
Transformations of the molecular variables in methylamine.

E	***a*** ≡ (123)(45)	***b*** ≡ (23)(45)*
χ	$\pi + \chi - 2\pi p/(6m)$	$\pi - \chi$
ϑ	ϑ	$\pi - \vartheta$
φ	φ	$\pi + \varphi$
τ	$\tau - 2\pi/6$	$-\tau$
γ	$-\gamma$	γ

where n is the ordinal number of a configuration which interacts with the configuration number 1. In other words, the interaction from framework $n = 1$ [133] does not involve any tunneling motion. The subsequent subscripts $n = 2, 4, 6\ldots$ correspond to tunneling of the NH_2 inversion, whereas $n = 3, 5, 7\ldots$ to torsional motion of the CH_3 group. As mentioned earlier, tunneling from position 1 to 2 involves inversion of the amino group followed by an internal rotation of the methyl group by 60°, and tunneling from conformation 1 to 3 corrseponds to an internal rotation of the methyl group by 120°. The effective terms of the Hamiltonian in Eq. (1) include $\Delta K = 0, \pm1, \pm2, \pm3, \pm4$ operators. The coefficients h, f, g, d, p, r, s are in dependence of the vibrational coordinates. They are multiplied by the rotational operators.

3.3. Spectrum of methylamine

Methylamine has been extensively studied by many experimentalists and its internal rotation and inversion barrier heights were determined by microwave spectroscopy, infrared experiments, or electron diffraction methods [137–142].

3.3.1. Ground vibrational state

There were many experimental studies of methylamine in cm-wave range performed in the fifties of the previous century [143–146] which were reviewed together with papers from the seventies [138,147] by Ohashi et al. [148] in 1987 and supplemented by far-infrared data covering a range from 4.6 to 90 GHz. Many experimental studies on methylamine involved millimeter- and submillimeter-wave ranges [149,150]. In one of them, Kręglewski et al. performed measurements allowing the determination of precise hyperfine constants [151]. Two important contributions were made by Ilyushin and Lovas [152] and Motiyenko et al. [153] which concerned the rotational spectrum of methylamine in its ground vibrational state. These studies summarized all available previous

$$H = \sum_{n=1}^{3m} H_n = \sum_{n=1}^{3m} \left\{ \begin{array}{c} h_n + h_{nj}P^2 + h_{nk}P_z^2 + h_{njj}P^4 + h_{njk}P^2P_z^2 + h_{nkk}P_z^4 + \\ f_n\left(P_+^2 + P_-^2\right) + g_n\left[i\left(P_+^2 - P_-^2\right)\right] + d_n\left(P_+^4 + P_-^4\right) + p_n\left[i\left(P_+^4 - P_-^4\right)\right] + \\ (r_{n+}P_+ + r_{n-}P_-) + [s_{n+}(P_zP_+ + P_+P_z) + s_{n-}(P_zP_- + P_-P_z)] \end{array} \right\} 2cos[(n-1)\rho\tau] + \sum_{n=2}^{3m} 2iq_nP_zsin[(n-1)\rho\tau] \quad (1)$$

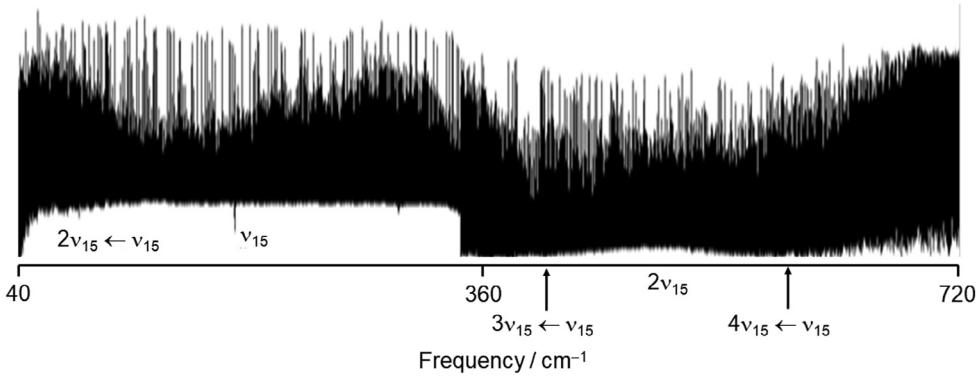

Fig. 11. The high-resolution infrared spectrum of methylamine in the range 40–720 cm^{-1}.

data covering the frequency range up to 500 GHz and 2.6 THz, respectively. The Hougen-Ohashi approach proved to be very accurate and allowed the fitting of all available data to the experimental precision [150,154].

3.3.2. The torsional states

Apart from the ground vibrational state of methylamine, there were numerous studies on the excited torsional states as well as the wagging state. Ohashi et al. studied the far-infrared spectrum in the region of the first excited torsional state, which corresponds to 40–350 cm^{-1} [154]. In this work, a number of rotational transitions were identified and fitted successfully using the Ohashi-Hougen formalism developed for methylamine [133] which was extended by adding $\Delta K = \pm 1$ operators to analyze the microwave spectrum from 7 to 90 GHz of the first torsional state [155]. The new microwave data were combined with previously obtained microwave transitions as well as the far-infrared lines and fitted using the extended tunneling-rotational Hamiltonian. Since the analysis of the first torsional state of methylamine was incomplete, additional measurements were taken by Gulaczyk et al. [156] and much more transitions were assigned and fitted globally together with all previous data. The global fit was performed using the group theoretical formalism of Ohashi and Hougen [133,155] which was further extended by adding subsequent operators, $\Delta K = \pm 3$ and 4, achieving an unitless standard error of 3 for microwave data and about 2 for rotational infrared data and for rovibrational data. Accurate rovibrational energy levels were calculated for the first excited torsional state of methylamine (ν_{15}) and then used in further analyses involving its hot bands.

The second excited torsional state of methylamine ($2\nu_{15}$) was also studied extensively, first in 1989 by Oda and Ohashi [157]. The analysis covered the torsional hot band (ν_{15} = 2–1) and infrared rotational transitions of the second torsional state. Since the assigned transitions overlapped with rotational lines in the ground state (ν_{15} = 0–0), in the first torsional state (ν_{15} = 1–1) and also with the overtone transitions (ν_{15} = 1–0), it was not possible to assign more transitions in the second excited torsional range. Consequently, the fit results obtained from the same group theoretical formalism used for the ground and the first torsional states were not sufficiently good, and the inversion tunneling splitting parameters could not be deduced. More information on the second torsional band (ν_{15} = 2–0) was obtained from the far-infrared Fourier-transform spectrum of methylamine in the region of 340–640 cm^{-1} [158]. Still, the number of transitions in the second overtone was not satisfactory and instead of a global fit, individual sub-bands were independently fitted to polynomials. In this analysis, some series of lines for the third and fourth excited torsional bands were also assigned, i.e. for ν_{15} = 3–1 and ν_{15} = 4–1, respectively. A complete structure of the second torsional state of methylamine was presented by Gulaczyk et al. [159] where rovibrational transitions belonging to the overtone band ν_{15} = 2–0 as well as to the hot torsional band ν_{15} = 2–1 were assigned and fitted to a theoretical model based on the Hougen-Ohashi formalism with a standard deviation of 0.006 cm^{-1}. Fig. 11 shows the high-resolution infrared spectrum of methylamine from 40 to 720 cm^{-1}. Although the range for the second torsional band is narrower, i.e. 340 to 720 cm^{-1}, this spectrum extends from 40 cm^{-1}, since the hot band ν_{15} = 2–1 was also the subject of the study. In the range of the spectrum given in Fig. 11, the hot band ν_{15} = 2–1, the first overtone ν_{15} = 1–0, the hot band ν_{15} = 3–1, the second overtone ν_{15} = 2–0, and the hot band ν_{15} = 4–1 are indicated.

Recently, Gulaczyk and Kręglewski reported a study on infrared rotational spectrum of methylamine, in which the ground state as well as the first and second excited torsional states were reanalyzed [160]. More infrared rotational lines were found in the region from 40 to 360 cm^{-1}, assigned, and fitted within each state, including all available microwave data. The results of these analyses were satisfactory, although deteriorating with higher states. The unitless standard error of the fit for the ground state with 78 parameters, $K \leq 20$, and $J \leq 50$ was less than 1. The respective values for the first excited state are 89 parameters, $K \leq 20$, $J \leq 45$, about 2 for rotational infrared data, rovibrational data, and microwave data; and for the second excited torsional state 95 parameters, $K \leq 14$, $J \leq 40$, 3.2 for rotational infrared data, 8.5 for overtone band data and for hot band data. The deviation of the fit for the second torsional state is three times smaller than in previous analysis [159] but still worse than for the first torsional state. Despite the increasing number of parameters with each state, it is not possible to fit the spectral data for the torsional excited states within experimental accuracy, probably because the group theoretical formalism has reached its limit. Another theoretical approach, called the "hybrid" approach, was proposed by Kleiner and Hougen [161]. In this approach, the $-NH_2$ wagging motion is treated by a tunneling formalism, while the $-CH_3$ internal-rotation motion by the usual torsion-rotation Hamiltonian using an explicit kinetic energy operator and potential energy function for that part. All the torsional states corresponding to the same umbrella-motion quantum number simultaneously can be fitted together. Currently, the ν_t = 1–1 microwave measurements, which were quite limited so far, have been extended, and present results on the fitting of already published far-infrared data from ν_t = 1–0 are encouraging with unitless standard deviation around 3 and 5 for ν_t = 0–0 and 1–1 microwave measurements and 1.6 for the far-infrared measurements mentioned above [162].

3.3.3. The inversion state

Tunneling-rotational levels of the first excited inversion state (ν_9 wagging) of methylamine were analyzed for the first time in

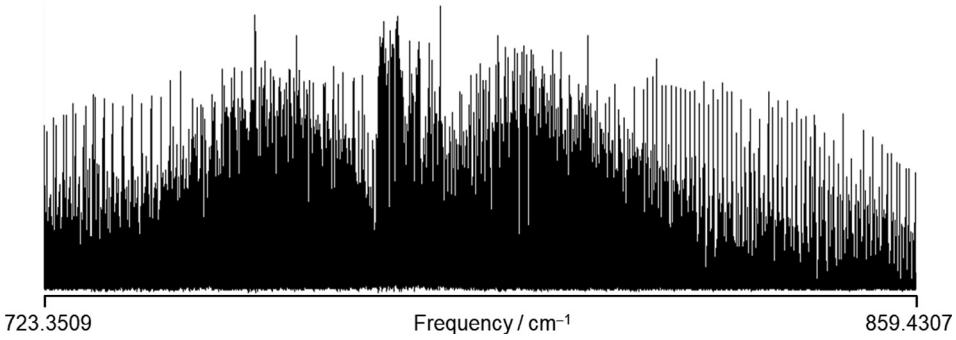

Fig. 12. The high resolution infrared spectrum of the wagging band ν_9 of methylamine.

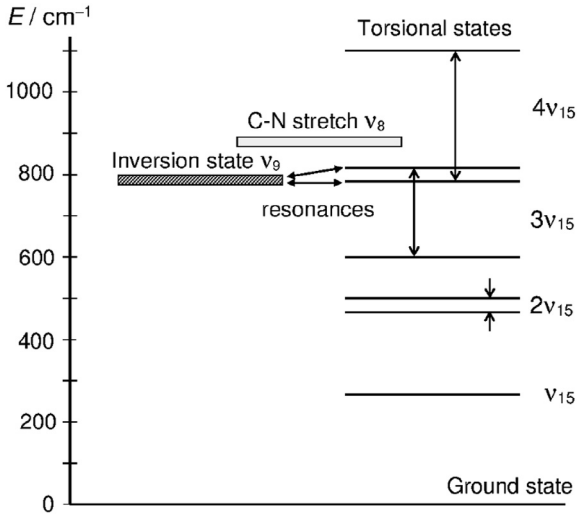

Fig. 13. A scheme of inversion-torsional energy levels of methylamine.

1992 [163]. The wagging band has a hybrid structure including parallel and perpendicular components, which is further split due to inversion and internal rotation of a molecule. The spectrum of the ν_9 wagging band stretches from 640 to 960 cm^{-1} as presented in Fig. 12. Like other parts of the infrared spectrum of methylamine, it is also very dense and overlapped. The results of the analysis performed by Kręglewski and Winther were satisfactory, although some series of lines were missing [163]. Sztraka et al. also studied the wagging band involving another approach [164] but some problems still remained.

Gulaczyk et al. [165] reinvestigated the inversion band of methylamine considering the resonances between the ν_9 wagging state and neighboring states. The most common perturbations arise from Fermi-type resonance and/or Coriolis interactions. As a result of perturbation, the so-called intensity borrowing may occur. It means that if the perturbing state (dark state) is of low intensity, but in interaction with a more intense state (bright state), the dark state borrows the intensity from the bright state while mixing and becomes visible in the spectrum. Perturbations manifest themselves in the spectrum with series of lines being shifted locally or globally.

Fig. 13 visualizes the energies of inversion-torsional states of methylamine. The inversion state could interact with three states: The C-N stretching ν_8, the third excited torsional $3\nu_{15}$, and the fourth excited torsional $4\nu_{15}$ states. The torsional states $3\nu_{15}$ and $4\nu_{15}$ show large torsional splittings that increase with the excitation. In fact, for the third excited state, only the upper part would take place in the resonance with the inversion state, whereas for the fourth excited state only the lower part participates. Reassignments of the wagging band resulted in a standard deviation of 0.018 cm^{-1}. Many missing lines were identified, even those that were perturbed, and a $K = 0$ series of B symmetry was shifted by 4 cm^{-1}. The perturbation turned out to arise from the fourth excited torsional state rather than the third torsional as believed earlier. In Ref. [166] Gulaczyk and Kręglewski reported that only states of the same symmetry regarding the reflection in the symmetry plane of the NH_2 group can interact through the Fermi resonance, satisfied by the fourth excited torsional state. The third torsional state can only cause Coriolis interactions. In order to obtain a better description of the wagging state, an effective Hamiltonian for inversion-torsional coupling should be built, which would take into account explicitly all interacting states.

3.3.4. The C-N stretching state

The C-N stretching band of methylamine (ν_8) was recorded in the high-resolution infrared spectrum from 960 to 1200 cm^{-1}. Fig. 14 shows a part of this band whose lines are strongly overlapped and of rather weak intensities. In Fig. 13, the C-N stretching

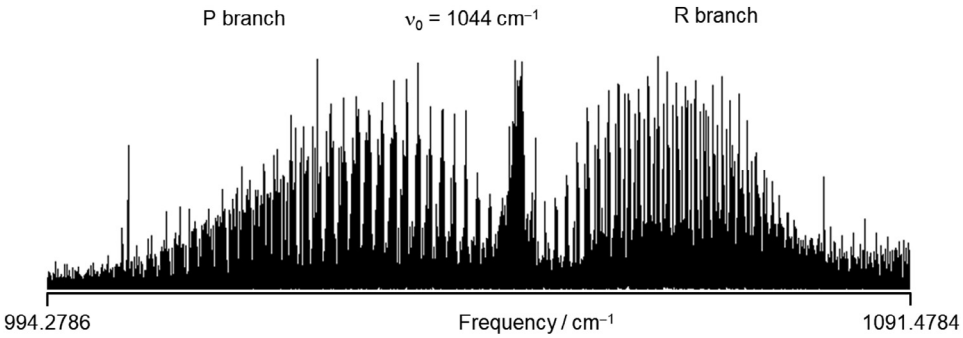

Fig. 14. The high resolution infrared spectrum of the ν_8 C-N stretching band of methylamine.

state is located above the inversion and the fourth torsional states, i.e. it might be perturbed by one of them. The analysis of this state was performed independently at the same time by Gulaczyk et al. [167] and by Lees et al. [168]. Most of the assigned lines in the C-N stretching band have been confirmed by ground state combinations differences and are consistent with the experimental laser lines [169–171].

Apart from transitions belonging to the ν_8 state, we observed transitions of another state in the studied region. They were assigned to the $K = 4$ series of $E_{2\text{-}1}$ symmetry of a perturbing (dark) state. To verify possible resonances of methylamine in the excited states, the torsion-inversion-rotational energy levels were calculated for some selected $J = K$. The values were obtained from a two dimensional potential surface [131]. A diagram of the energies of the inversion-torsional states are presented in Fig. 15. The states that were taken into account are the excited torsional states ν_{15}, $2\nu_{15}$, $3\nu_{15}$, $4\nu_{15}$, the excited inversion state ν_9, the combination state $\nu_9 + \nu_{15}$, and the C-N stretching state ν_8. In the energy ladders for $K = 4$, the best candidates for a "dark" state are the combination state $\nu_9 + \nu_{15}$ and the fourth excited torsional state $4\nu_{15}$. As mentioned above, to identify which state is the perturber, it is necessary to consider symmetry rules for the interacting states [166]. Thus, for a Fermi-type resonance only states of the same symmetry (A'–A' or A"–A") can be taken into account. The symmetry of the C-N stretching state is A' and therefore, the perturber should be the fourth excited torsional state. The fit was performed using the Ohashi-Hougen single state model with the final standard deviation of 0.04 cm^{-1} [167]. In the study by Lee et al. [168] high-resolution laser sideband and Fourier transform synchrotron spectroscopy were used, then applying a phenomenological Fourier series model to fit the ground and C-N stretch origins. Some anharmonic resonances with $\nu_t = 4$ (the fourth excited torsional state) were observed and identified partially. From *J*-localized level-crossing resonances, the interaction coupling constants could be determined.

Although many transitions could be assigned and perturbations from several resonances (Fermi and Coriolis) were analyzed, still many overlapped lines remained unidentified in the Fourier transform spectrum for the C-N stretching band. In a study by Sun et al. [172] new experimental results were reported using microwave sidebands of CO_2 laser lines as frequency-tunable infrared sources in a sub-Doppler spectrometer. Many blended and unresolved *K*-doublet lines in Doppler-limited spectra had been separated to confirm and extend the previous set of transitions [167,168].

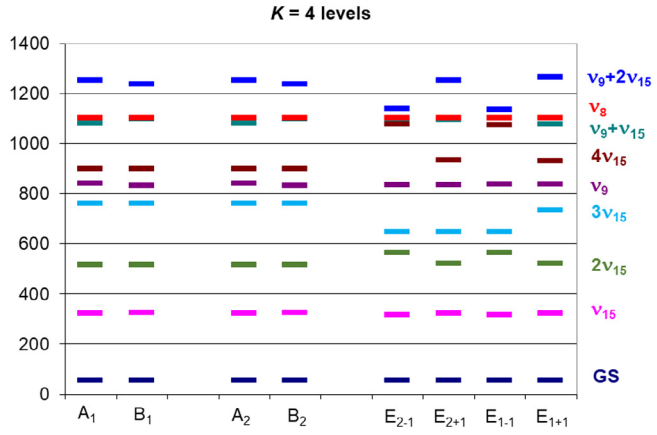

Fig. 15. Energy level schemes of methylamine with $J = K = 4$ for different symmetry species. GS: ground state; ν_{15}, $2\nu_{15}$, $3\nu_{15}$, $4\nu_{15}$: excited torsional states; ν_9: excited wagging state; ν_8: C-N stretching state; $\nu_9 + \nu_{15}$, $\nu_9 + 2\nu_{15}$: combination states.

In newer contributions, the high resolution infrared spectrum of methylamine has been studied in the regions of the C-H stretching [173,174] and NH_2 scissors modes [175]. In the ν_{11} CH-stretch region (2965– 3005 cm^{-1}) recorded using slit-jet direct absorption spectroscopy with a resolution of 0.0025 cm^{-1}, about 600 lines were assigned for $K \leq 2$ and the A, B, E_1, and E_2 symmetries. The analysis of the spectrum revealed two qualitative differences in the energy level pattern concerning the vibrational ground state and relative to available data on the NH_2 wagging and C-N stretch vibrations [173]. Two torsion-inversion tunneling models were presented for the C-H stretch vibrationally excited states in the G_{12} family of molecules like methylamine. One model is a group theoretical treatment starting from the symmetric rotor methyl C-H stretch vibrations. The other one is an internal coordinate model including the local-local C-H stretch coupling. Both models yield predicted torsion-inversion tunneling patterns of the four symmetry species aforementioned in the C-H stretch excited states [174]. Recently, a rotationally resolved spectrum of methylamine was recorded at room temperature in the region of 1540–1710 cm^{-1} with a resolution of 0.001 cm^{-1} using a White-type multipass cell device coupled to the Bruker IFS 125 HR Fourier transform spectrometer implemented on the AILES beamline at the SOLEIL synchrotron. A low temperature high resolution spectrum in the 1622.5–1655.6 cm^{-1} range of *Q* and *R* branches of the NH_2 scissors (ν_4) band was recorded using a quantum cascade laser spectrometer, and has been assigned with about 2200 transitions for *K* from 0 to 6 [175].

3.4. Theoretical studies

Methylamine is of great interst for both experimentalists and theoreticians. A wealth of experimental data is available to verify theoretical results of methylamine, which is a small molecule from today's theoretical point of view, now suitable to be studied with high level quantum chemical methods. Indeed, methylamine was extensively studied theoretically [142,176–182]. Many theoretical studies on the inversion-torsional spectrum were performed, where two-dimensional Hamiltonians were solved variationally to obtain the low vibrational energy levels [178,183,184]. The computed energy levels were compared with those estimated by Kręglewski using experimental data [62,185]. Recently, Senent [186] applied explicitly correlated coupled cluster methods (CCSD(T)-F12) to calculate the far infrared spectra of methylamine. A three-dimensional Hamiltonian was applied and three coordinates were considered explicitly, i.e. the NH_2 wagging, the HNH bending, and the CH_3 torsion.

3.5. Methylamine complexes

The lone pair of electrons on the nitrogen atom of methylamine, as shown in Fig. 16, can facilitate the formation of various types of complexes with metal ions [47,48]. Applications of coordination compounds involving methylamine are as wide spread as they can be. Some of the complexes are widely used in supramolecular chemistry as polymeric networks [49] many of which are based on

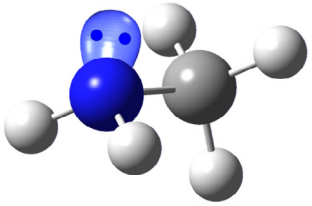

Fig. 16. The structure of methylamine with its lone pair of electrons.

multidentate flexible ligands, featuring different conformations such as boxes, helices etc. depending on the properties of the metal ions. A lot of interest was focused on clusters of alkali metal atoms with ammonia molecules because they dissolve easily in liquid ammonia [50] to form colorful and highly conducting solutions. The alkali metals can also dissolve in ammonia derivatives such as methylamine. Many studies were performed in order to describe the change of ammonia into methylamine on the alkali cation and solvated electrons. For example, the first infrared spectra of Li $(NH_2CH_3)_n$ for n = 3–5 clusters were recorded and compared with theoretical results from *ab initio* calculations [51] proving that the first solvation shell can provide space for up to four methylamine molecules on a tetrahedral coordination. The methyl groups move away from the lithium atom to avoid steric repulsion.

Another important applications of methylamine complexes are surface coatings, adhesion, catalysis, and corrosion inhibition, where methylamine is bound to the surface through its lone pair of electrons. Adsorbed methylamine has been studied on surfaces of nickel and chromium at 300 K using electron energy loss spectroscopy (EELS) [187,188]. Studies of adsorbed methylamine on Pt surface also exist [189,190]. Perovskite photovoltaics used in solar cells are also of great interest. Recently, Bogachuk et al. showed a connection between the interatomic bonding in the methylamine-PbI_3 complex during liquefaction and recrystallization and the crystal morphology as well as the lifetime of photo-generated carriers in mesoporous layer and planar structures [191].

Methylamine complexes play an important role in medicine also. It was investigated that solubility and anticancer activity of *cis*-platin can be improved by methylglycine and methylamine ligands against human breast cancer [52]. Two water-soluble platinum (II) complexes *cis*-[$Pt(NH_2CH_3)_2(CH_3$-gly)]NO_3 and *cis*-[$Pt(NH_3)_2(CH_3$-gly)]NO_3 were synthesized and successfully characterized by different spectroscopic methods. These complexes were used for testing against the human breast adenocarcinoma cell line. Both complexes turned out to have satisfactory anticancer activity. Methylamine can be also a part of luminescence materials obtained from trivalent lanthanide ions with the ligands tris((1H-benzo[d]imidazol-2-yl)methyl)amine [192].

4. Hydrazine

Hydrazine, NH_2NH_2, is a reducing agent and reactive base used in industrial, pharmaceutical, as well as medical applications. Among those, hydrazine and its derivatives possess antidepressant properties. They inhibit the enzyme monoamine oxidase which catalyzes the inactivation and deamination of some stimulatory neurotransmitters. Hydrazine is an inorganic compound well-known with its homogeneous non-metal character. Moreover, hydrazine has been found in human liver and kidney tissues, and has also been detected in biofluids such as urine and blood. Within the cell, hydrazine is mainly situated in the cytoplasm. Hydrazine is used for electrolytic plating of metals on glass or plastic and as a chemical intermediate for the synthesis of countless chemicals with N-N bonds. It is known also as a rocket propellant, as a boiler feed water deoxygenating agent, and used widely in the manufacture of foamed plastics, biodegradable pesticides, insecticides, fungicides, or herbicides. Hydrazine is of particular interest in coordination compounds, since there are various ways in which hydrazine can be bonded to the metal: monodentate, bridging, and bidentate [57].

4.1. Internal dynamics and symmetry of hydrazine

Like methylamine, hydrazine is a non-rigid molecule, which has been of great interest for spectroscopists and theoreticians for decades. Its dynamics are governed by three LAMs, which are two inversions of the amino groups $–NH_2$ and an internal rotation (torsion) of the two amino groups around the N-N bond. These three LAMs generate various tunneling splitting patterns in different vibrational states of a molecule. Each of them features two equivalent equilibrium conformations, leading to 8 non-superimposable configurations. The $–NH_2$ wagging motion at each end of the molecule is described by the inversion coordinates γ_1 and γ_2. The torsional motion is described by the rotational angle τ. γ_1 and γ_2 are angles between the HNH angle bisector and the axis that passes through the local centers of mass of two NH_2 groups. τ is a half of an angle between two NH_2 groups assuming the inversion coordinates equal zero. Fig. 17 presents two projections of a hydrazine molecule defining the inversion coordinates and the torsional coordinate in the molecular axis system. The LAM coordinates are curvilinear.

The equilibrium structure of hydrazine belongs to the point group C_2 [29] which comprises two symmetry operations. The extended permutation-inversion group for hydrazine is $G_{16}^{(2)}$. This double Longuet-Higgins permutation-inversion group is generated by four symmetry operators *a*, *b*, *c*, and *d*, where the last operation *d* is only responsible for a double group. The other symmetry operators are described by the permutation-inversion operations as *a* = (34)(1526)*, *b* = (34)(15)(26), and *c* = E* (for atom numbering, see Fig. 17). The symmetry group for hydrazine is of order 8 and consists of eight permutation operations [193]. Longuet-Higgins proposed a symmetry group of order 16 [134] containing the eight permutations of nuclei and eight permutation-inversion operators. A permutation-inversion group of order 32 was introduced by Papoušek et al. [194] and Merer and Watson [195]. Thus, the 16-element group is a subgroup of the double group $G_{16}^{(2)}$, the pure permutation group G_8 is a subgroup of G_{16}, and the equilibrium geometry point group C_2 is a subgroup of G_8. The character table of the group $G_{16}^{(2)}$ is presented in Table 3.

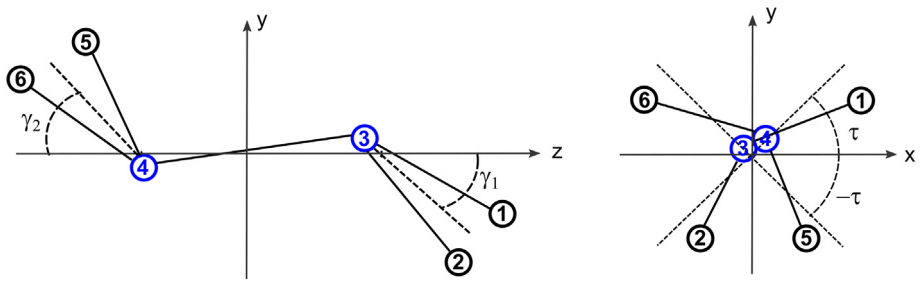

Fig. 17. The inversion coordinates γ_1 and γ_2, the torsional coordinate τ, and the molecular axis system of hydrazine.

Table 3
Character table of the double permutation-inversion $G_{16}^{(2)}$ group.

	e	d	a^2	a^2 d	c cd	a^2c a^2cd	b a^2b	bd a^2bd	bc a^2bc	a^2b bcd	a a^3 ad a^3d	ac a^3c acd a^3cd	ab a^3b abd a^3bd	abc a^3bc abcd a^3bcd
A_{1g}^{+}	1	1	1	1	1	1	1	1	1	1	1	1	1	1
A_{2u}^{+}	1	1	1	1	1	1	−1	−1	−1	−1	1	1	−1	−1
A_{1u}^{-}	1	1	1	1	−1	−1	1	1	−1	−1	1	−1	1	−1
A_{2g}^{-}	1	1	1	1	−1	−1	−1	−1	1	1	1	−1	−1	1
B_{1g}^{+}	1	1	1	1	1	1	1	1	1	1	−1	−1	−1	−1
B_{2u}^{+}	1	1	1	1	1	1	−1	−1	−1	−1	−1	−1	1	1
B_{1u}^{-}	1	1	1	1	−1	−1	1	1	−1	−1	−1	1	−1	1
B_{2g}^{-}	1	1	1	1	−1	−1	−1	−1	1	1	−1	1	1	−1
E^{+}	2	2	−2	−2	2	−2	0	0	0	0	0	0	0	0
E^{-}	2	2	−2	−2	−2	2	0	0	0	0	0	0	0	0
E_1	2	−2	2	−2	0	0	2	−2	0	0	0	0	0	0
E_2	2	−2	2	−2	0	0	−2	2	0	0	0	0	0	0
E_g	2	−2	−2	2	0	0	0	0	2	−2	0	0	0	0
E_u	2	−2	−2	2	0	0	0	0	−2	2	0	0	0	0

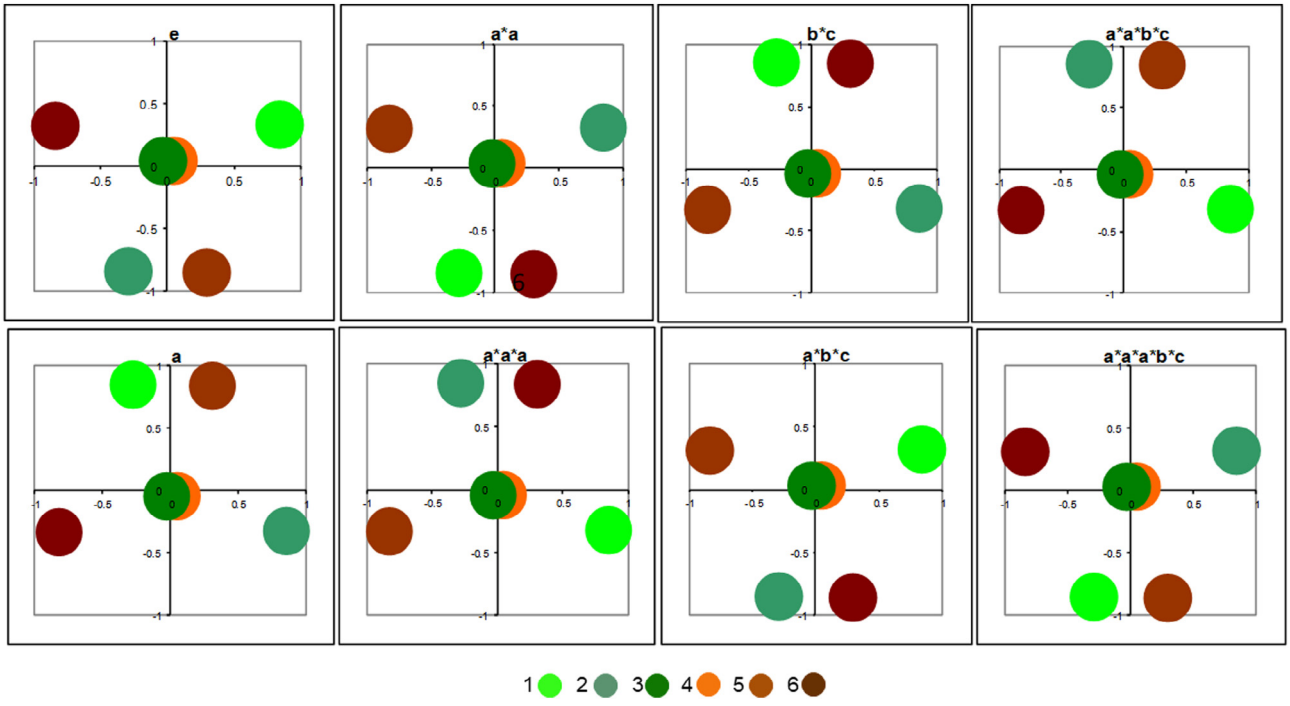

Fig. 18. The 8 non-superimposable frameworks of hydrazine. The colors of the circles represent the atoms with their numbering as indicated in Fig. 17.

4.2. Tunneling formalism in hydrazine

The slow tunneling formalism was developed for the first time in 1981 by Hougen [196] based on the theory proposed by Kasuya [29]. A phenomenological Hamiltonian operator was derived for fitting the rotational energy levels of the vibrational ground state. Hydrazine has 8 non-superimposed frameworks as depicted in Fig. 18. The molecule tunnels from one framework to another. However, most of its time is spent in the neighborhood of conformational vibrating. This is an important assumption of the slow tunneling formalism, since splittings caused by the tunneling motion should be relatively small compared to differences between the vibrational energy levels.

Each non-superimposable conformation possesses its inversion-torsional function. Therefore, a vibration–rotation basis set of 16 functions (Ψ_{nA}, Ψ_{nB}) can be obtained by multiplying a vibrational wave function located at the equilibrium conformation by each of the two components (A or B) of a rotational K-doublet. The explicit form of inversion-torsion functions does not matter, only their symmetry properties are important. Combinations of inversion-torsion functions localized in 8 non-superimposable configurations belong to the symmetry species $A_{1g}^{+}, A_{1u}^{-}, B_{1g}^{+}, B_{1u}^{-}, E^{+}, E^{-}, E_g, E_u, E_1$. The rotational functions are of $A_{1g}^{+}, A_{2g}^{-}, B_{1g}^{+}, B_{2g}^{-}, E_g$ symmetry. The symmetry of the resulting rotation-inversion-torsional functions are $A_{1g}^{+}, A_{2g}^{-}, B_{1g}^{+}, B_{2g}^{-}, A_{1u}^{-}, A_{2u}^{+}, B_{1u}^{-}, B_{2u}^{+}, E^{+}, E^{-}$, respectively.

The rovibrational effective Hamiltonian for hydrazine is expressed by:

$$H = \sum_{n=1}^{8} H_n$$
$$= \sum_{n=1}^{8} h_{nv} + h_{nj}P^2 + h_{nk}P_z^2 + h_{njj}P^4 + h_{njk}P^2P_z^2 + h_{nkk}P_z^4 + f_n\left(P_+^2 + P_-^2\right) + g_n\left[i\left(P_+^2 - P_-^2\right)\right] + q_nP_z + d_n\left(P_+^4 + P_-^4\right) + p_n\left[i\left(P_+^4 - P_-^4\right)\right] + (r_{n+}P_+ + r_{n-}P_-) + [s_{n+}(P_zP_+ + P_+P_z) + s_{n-}(P_zP_- + P_-P_z)] \quad (2)$$

In the tunneling model, LAMs take place from any of the frameworks in Fig. 18 to any other. The subscript n in Eq. (2) indicates the number of a framework. The matrix elements of the Hamiltonian can be presented in the form $\langle 1|H|n\rangle$, where n = 1 corresponds to no tunneling motion, n = 2 to inversion of both NH_2 groups, n = 3 to internal rotation, n = 4 to inversion of both amino groups and internal rotation, n = 5 to inversion of one amino group, n = 6 to inversion of the other amino group, n = 7 to inversion of one of the amino group and internal rotation, and n = 8 to inversion of the other amino group and internal rotation. Tunneling of n = 5 and n = 6 along with n = 7 and n = 8 are equivalent, thus only matrix elements with n = 1, 2, 3, 4, 5, and 7 can be considered explicitly. The molecular parameters h_{nv}, h_{nj}, h_{nk}, f_n, g_n, q_n, d_n, p_n, r_n, s_n in Eq. (2) are multiplied by the appropriate rotational operators. The Hamiltonian matrix is constructed from products of inversion-torsion and rotational function.

Later, Ohashi and Hougen [197] rederived the results obtained earlier for hydrazine using a tunneling formalism of Hougen [196]. The later approach considers tunneling between 16 minima instead of eight non-superimposable frameworks. In this separate treatment, only the vibrational part of the tunneling problem was taken into account in the first step, then multiplying the vibrational eigenfunctions with the symmetric top rotational wavefunctions. This method seems to be easier, but has some drawbacks. In the vibration–rotation approach a basis set could consist of one vibrational wavefunction for each of the frameworks, while in the separate approach a basis set has to contain two vibrational wavefunctions for each of the frameworks, which gives 16 vibrational wavefunctions.

4.3. Spectroscopic studies

Many spectral regions of hydrazine have been studied over the years. The low resolution infrared spectrum was recorded in 1952 [198]. From this analysis, it was possible to determine the position of the symmetric inversion band. The ground vibrational state observed in the microwave region from 6 to 133 GHz was extensively analyzed [29,199] for which the group-theoretical formalism of Hougen [196] was developed and yielded a satisfactory global fit.

A number of infrared data have also been analyzed. The first excited torsional band (ν_7) of hydrazine was studied in the range from 200 to 450 cm^{-1} [200]. This work aimed to check whether the group-theoretical formalism applied earlier for the ground state, where the inversion and torsional splittings are rather small, could be successfully used for the state with much larger torsional splittings. A global least-squares fit was performed considering the far-infrared data together with the ground state microwave data [199]. The fit was satisfactory, although some parameters could not be determined for the excited torsional state, probably because not enough transitions were observed.

The infrared spectrum of hydrazine was also studied in the frequency range of the second excited torsional band from 580 to 750 cm^{-1} [201,202]. The main interest of this analysis was to determine how the splittings caused by the inversions and torsion change with excitation of two quanta. It turned out that indeed the parameters responsible for the *trans*-tunneling motion had increased significantly with torsional excitation. The h_{3v} parameter (see Eq. (2)) was about 100 times larger than that of the first excited state and almost 35 000 times larger than that of the ground state. A global fit of the assigned transitions for the ν_7 = 2–0 yielded a decent result.

The inversion motions in hydrazine can be in-phase, then the vibration is symmetric (symmetric wagging, ν_6), or out-of-phase and the vibration is antisymmetric (antisymmetric wagging, ν_{12}). A number of analyses of the antisymmetric inversion (amino-wagging) state of hydrazine were performed [203–208]. Tsuboi et al. [206] determined the energy level structure for the K' = 1 rotational state of the antisymmetric amino-wagging band along with some molecular parameters. Jones and Takami [205] used infrared-microwave double resonance to determine a number of parameters for the second excited torsional state and confirmed that the inversion splitting changed significantly on the excitation of the antisymmetric amino-wagging. The inversion splitting in the ground vibrational state is about 0.5 cm^{-1}, while in the first excited state of the antisymmetric amino-wagging vibration it is 13 cm^{-1}. Further analysis with additionally assigned lines of the antisymmetric amino-wagging band ν_{12} of hydrazine was performed by Ohashi et al. [207]. A global fit was not successful, and only individual sub-band fits were achieved, showing that the group-theoretical formalism of Hougen [196] was not able to properly represent the transitions belonging to the ν_{12} state, probably because some perturbations might occur in the antisymmetric amino-wagging state. At that time, there were several candidates for an interaction with the ν_{12} state. Among these potential "dark" states were two fundamental vibrations: the N-N stretching vibration (ν_5) and the symmetric amino-wagging vibration (ν_6). The third excited torsional state $3\nu_7$ was also considered, since the torsional splitting in this state was estimated to be very large and some levels of $3\nu_7$ could lie close to the ν_{12} state.

Another spectrum of hydrazine was recorded in the range from 729 to 1198 cm^{-1} [208] to complete the assignment of the ν_{12} band needed to enable the analysis of the symmetric amino-wagging state, ν_6, which partly overlaps with the ν_{12} band. The effective parameters were obtained separately for each K value using the Hougen-Ohashi Hamiltonian while also applying the expressions developed by Ohashi and Matsue [209].

The symmetric amino-wagging ν_6 band of hydrazine was assigned and analyzed for the first time in 2008 [210]. It turned out that the symmetric amino-wagging state with a band center at 780 cm^{-1} was strongly perturbed globally by one of the neighboring states. Some of the lines were shifted by 10 cm^{-1}. Fig. 19 shows the scheme of inversion-torsional energy levels, indicating that ν_{12} lies closest to ν_6. It was not possible to consider the interaction between the symmetric and antisymmetric wagging states, since two states being in a Fermi-type resonance should have the same symmetry with respect to the rotation around the C_2 axis of a molecule. Such conclusion has been drawn from a study on the effective Hamiltonian for the coupling between inversion-torsion states of hydrazine [211]. The symmetric wagging is of A symmetry, whereas the antisymmetric wagging is of B symmetry. The state of A symmetry is the third excited torsional $3\nu_7$. Thus, these two states were considered to be in a strong resonance. Since the global fit using the Hougen formalism gave a standard deviation much larger than the experimental accuracy, fits for individual K values were run and the coupling terms between the $3\nu_7$ and ν_6 states were obtained. Not all the series were identified in the symmetric wagging band, implying that there are still some unidentified perturbations.

While analyzing the rotational structure of both wagging states, the lines of the N-N stretching band with a band center at

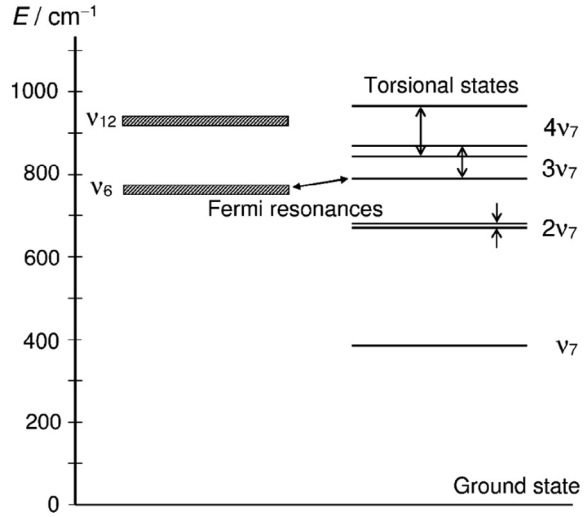

Fig. 19. A scheme of energy levels of the wagging-torsional states of hydrazine.

1077 cm^{-1} were observed in the spectrum of hydrazine [212]. Again, analysis by a global fit was not as good as individual fits for the *K* values, probably due to perturbations.

4.4. Theoretical studies

There are a series of theoretical studies for hydrazine [213–215]. Initially, the two-dimensional potential function for the inversion of the amino groups were calculated from a fit to the available spectroscopic data [213]. The barriers for the symmetric and antisymmetric wagging motions were obtained to be 3408 and 2016 cm^{-1}, respectively. Ref. [214] showed how information about the inversion-torsion potential can be retrieved from the rovibrational spectrum of hydrazine. The calculated inversion and internal rotation barriers were 2072 cm^{-1} and 934 cm^{-1}, respectively. From the inversion-torsional potential function, the energy including torsional and inversion splittings for the $3\nu_7$ state were calculated [210]. These energies and extrapolated parameters from the ν_7 and $2\nu_7$ torsional states were taken for the initial estimation of the parameters used for the $3\nu_7$ state in the effective Hamiltonian. In the study of Łodyga and Makarewicz, *ab initio* methods were used to calculate anharmonic frequencies and torsion-wagging multiplets of hydrazine [215]. Harmonic frequencies were calculated also by other theoreticians [216–219].

In conclusion, hydrazine draws much attention from its complex internal dynamics governed by three LAMs, causing difficulties in spectral assignment.

4.5. Hydrazine complexes

Hydrazine and its derivates have been of great interest to chemists, material scientists, and engineers for many years due to their wide applications in various fields. With two active nucleophilic nitrogens and four substitutable hydrogens, hydrazine is a good starting point for many derivatives like foaming agents for antioxidants, plastics, fungicides, herbicides, polymer chain-extenders, and cross-linkers. Hydrazine is also a good ligand and therefore, many complexes including a hydrazine molecule have been studied [220–227].

The *gauche* conformation of hydrazine has one NH_2 group twisted from the *trans* or *cis* positions. The vacant tetrahedral positions are occupied by two lone electron pairs in the sp^3 hybridization. They are the source of the nucleophilic and basic character of hydrazine. The free electrons of hydrazine are able to coordinate to

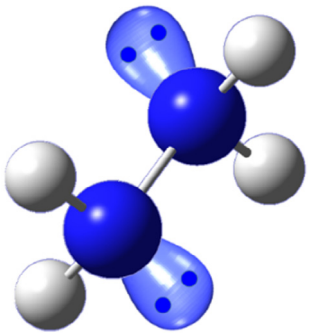

Fig. 20. Structure of a hydrazine molecule.

metal ions either as a monodentate or as a bridged bidentate ligand. It is noteworthy to mention a few metal hydrazine complexes including different anions like perchlorate, oxalate, sulfate, azide, nitrate, hydrazine carboxylate [54]. In most of these complexes, hydrazine acts as a bridged bidentate ligand, and only in some as monodentate. Fig. 20 presents the structure of hydrazine with its two pairs of free electrons and four substitutable hydrogen atoms.

The chemistry of hydrazine and its derivatives, including many different types of complexes, is rich. Belonging to the group of hydrazine compounds are its inorganic derivates, hydrazinium metal complexes, metal hydrazines, hydrazine salts, metal hydrazine carboxylates, and many others. Transition metal complexes with monodentate and bridging hydrazines are formed with various metals (Ag, Ca, Co, Cr, Cu, Er, Fe, Hg, Mn, Mo etc.) and anions (carbonate, halide, nitrate etc.) that have been synthesized and characterized [55–57]. Hydrazine, as a strong base, hydrolyzes in aqueous solution:

$$N_2H_4 + H_2O \rightarrow N_2H_5^+ + OH^- \quad (3)$$

$$N_2H_5^+ + H_2O \rightarrow N_2H_6^{+2} + OH^- \quad (4)$$

The $N_2H_5^+$ cation is called a hydrazinium cation and the $N_2H_6^{+2}$ cation is a hydrazonium cation. Free hydrazine, hydrazine hydrate, and monoprotonated hydrazine are all well-known ligands for coordination complexes with transition metals [228,229].

5. Secondary amine

The complex coupling between the inversion tunneling and the methyl torsion has made methylamine a challenging molecule which has been extensively studied and is still of great interest for both experimentalists and theoreticians. As mentioned in the introduction, this coupling occurs quite often, especially in primary amines where the inversion motion of the two hydrogen atoms in the amino group is always accompanied by the internal rotation of the entired amino group [53,61–63]. In only some molecules like dimethyl amine, CH_3-**NH**-CH_3, [230] ethyl methyl amine, CH_3-CH_2-**NH**-CH_3 [231,232] and diethyl amine, CH_3-CH_2-**NH**-CH_2-CH_3 [233] the inversion tunneling of the proton attached at the nitrogen atom is not coupled by internal rotation, at least in the vibrational ground state. Though the effects of internal rotation are present, origining from the two methyl groups in the molecules, the torsional barriers are sufficiently high, leading to much smaller splittings of about 10^{-5} relative to those caused by the tunneling motion.

Ammonia was extensively studied in the micron region, while methylamine and hydrazine were mainly observed in the infrared range. Nevertheless, microwave spectroscopy covers a much more suitable frequency domain to study the spectra of secondary

amines, being an analytical method well established to extract information on conformational structures of small to medium-sized organic molecules in the gas phase. The microwave spectra are conformational specific and enable the characterization of individual conformers of a molecule.

Atmospheric chemistry and astrophysics are two major research fields that employ microwave spectroscopy. For atmospheric chemistry, knowing the structures and dynamics of molecules existing in our atmosphere are of fundamental importance to understand the concepts of kinetical processes and climate [234] with a vast amount of research focusing on chemical compositions and direct changes on the radiative forcing of the atmosphere [235]. Within the lower troposphere, the spectra of smaller organic molecules lead to key information about the origin of such compounds, as demonstrated in the works of Blumestock et al. with the detection of unusual chlorine activation during the arctic winter [236]. Atmospheric research has been extended to other planets and within our solar system. Muhleman and Clancy have reported the rotational spectra of H_2O, CO, O_2, O_3, and H_2O_2 in the atmosphere of Mars, which helped for better knowledge of the water cycle and composition of the Mars atmosphere [237]. Many sizable organic compounds were also identified in the interstellar medium by rotational spectroscopy, for example the detection of methyl acetate and *gauche* ethyl formate in the Orion Nebula [238] followed by the detection of ethyl formate in the giant molecular cloud Sagittarius B2 near the center of the Milky Way Galaxy. An actively maintained list of all molecules detected in the interstellar medium can be found, e.g., at the Cologne Database for Molecular Spectroscopy (CDMS) website [239]. Among around 200 molecules detected in the interstellar medium or circumstellar shells [239] none of them are secondary amines, despite intensively been seeked for because of their importance in biology and chemistry. This might be explained by a lack of laboratory investigation of rotational spectra of those molecules, as pointed out in a recent review by Kleiner [240]. So far, the spectra of only three linear aliphatic secondary amines were studied by high resolution microwave spectroscopy, which are dimethyl amine [230] ethyl methyl amine [231,232] and diethyl amine [233]. Studies on extension to higher frequency range do not exist.

This class of molecules is particularly interesting for spectroscopic research because they feature a multitude of different effects that typically occur in the microwave region. As mentioned above, the terminal methyl groups undergo internal rotation that cause small fine splittings. Additionally, the ^{14}N nucleus causes a quadrupole hyperfine structure in the margin of few hundreds of kHz to several MHz. Finally, an effect which makes them of great interest for this review is the tunneling motion of the hydrogen atom attached to the nitrogen atom. This inversion tunneling causes the *c*-dipole moment component to change its sign, resulting in splittings from *c*-type transitions across the non-degenerate *s* and *a* symmetry species of all rotational levels. Such tunneling splittings of 2646.0 MHz, 1981.0 MHz, and 1521.5 MHz have been reported for dimethyl amine [230] ethyl methyl amine [231,232] and diethyl amine [233] respectively.

Results of the geometry optimizations reveal that all heavy atoms of the energetically most stable conformer of dimethyl amine, ethyl methyl amine, and diethyl amine are located in the *ab*-plane, as illustrated in Fig. 21. The hydrogen of the amino group can be on either side of this plane, resulting in two energetically equivalent structures which are enantiomers and have different signs of the *c*-dipole moment component (see also Fig. 21). The potential energy curve of the proton inversion process can be calculated by varying the angle $\gamma = \arccos\left(\frac{\overrightarrow{C_cN} \cdot \overrightarrow{NH}}{|\overrightarrow{C_cN}| \cdot |\overrightarrow{NH}|}\right)$ between the plane containing the heavy atoms and the amino-hydrogen bond within a range of 0° to about 90° due to symmetry. C_c denotes the center between the two carbon atoms binding to the nitrogen atom. The predicted energies can be parameterized to yield a potential energy curve with a double minimum similar to that of ammonia illustrated in Fig. 1. An example for diethyl amine is given in Fig. 22 [233]. The local maximum at $\gamma = 0°$ describes a planar sp^2 configuration of the nitrogen atom with the amino hydrogen and the neighboring carbon atoms being co-planar. Electron delocalization due to the lone electron pair makes this planar configuration, however, a transition state. Away from the two minima, the potential energy increases rapidly due to the close proximity of amino-hydrogen to the alkyl groups.

Similar to the energy levels of ammonia, the vibrational ground state splits into a lower symmetric *s* and a higher anti-symmetric *a* sublevel from the inversion motion of the amino hydrogen atom. Because the sign of the *c*-dipole moment component changes upon

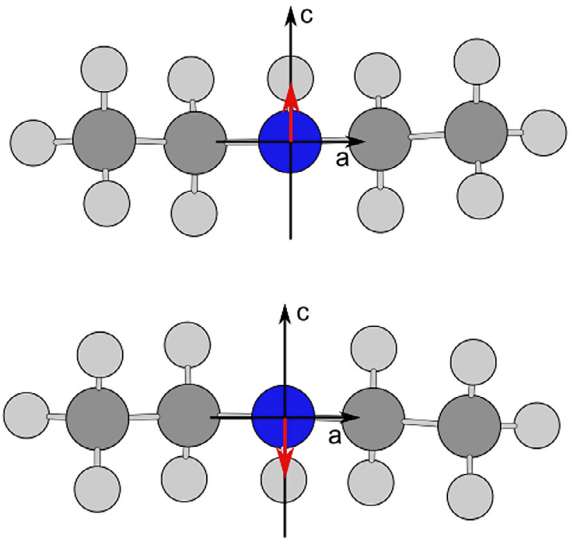

Fig. 21. The two equivalent equilibrium geometries of diethyl amine obtained by quantum chemistry which correspond to the two energy minima of the proton tunneling. The principal *a* and *c* inertia axes are given, indicating that the dipole component (red arrow) changes sign in *c* direction during the tunneling process.

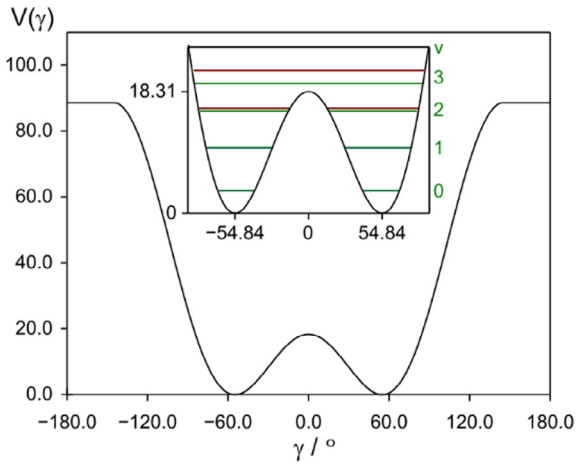

Fig. 22. The double minimum potential of the proton tunneling inversion process of diethyl amine. The inversion coordinate γ is defined as the angle between the NH bond and the NCC plane. The inset shows the inversion levels that split into an *s* and an *a* sublevel and the barrier height calculated from the v = 0 inversion splitting. Calculations were carried out as described in Ref. [233].

inversion, the selection rules $s \leftrightarrow a$ across the two symmetry species are obtained for *c*-type transitions. This means that a pattern of doubled *c*-type transitions appears in the spectrum, as illustrated in Fig. 23. The sign of the *b*-dipole moment component retains during the inversion process, maintaining the selection rules $s \leftrightarrow s$ and $a \leftrightarrow a$ within the two symmetry species for *b*-type transitions. To fit the microwave spectrum of these secondary amines, the following effective Hamiltonian can be used:

$$H = \sum_{v=0}^{1} |v\rangle(H_r + H_\Delta + H_{NQ})\langle v| + (|0\rangle\langle 1| + |1\rangle\langle 0|)H_c \quad (5)$$

$|0\rangle$ describes the *s* and $|1\rangle$ the *a* tunneling state. H_r contains the overall rotation and the quartic centrifugal distortion terms and can be described by Watson's S-reduced Hamiltonian in its I^r representation:

$$\begin{aligned} H_r &= AP_a^2 + BP_b^2 + CP_c^2 \\ &-D_J P^4 - D_{JK}P_a^2 - D_K P_a^4 + d_1 P^2\left(P_+^2 + P_-^2\right) + d_2\left(P_+^4 + P_-^4\right) \end{aligned} \quad (6)$$

where *A*, *B*, and *C* are the rotational constants, D_J, D_{JK}, D_K, d_1, and d_2 the quartic centrifugal distortion constants with P_+ and P_- being the step operators. The H_{NQ} term denotes the quadrupole coupling

$$H_{NQ} = \frac{1}{2I(2I-1)} \sum_{\alpha,\beta} \chi_{\alpha\beta}[I_\alpha, I_\beta]_+ \text{with} \chi_{\alpha\beta} = e\boldsymbol{Q}q_{\alpha\beta} \quad (7)$$

where $\boldsymbol{Q}$ is the nuclear quadrupole moment, $\chi_{\alpha\beta}$ are the tensor elements proportional to the elementary charge *e* and the electric field gradient tensor elements $q_{\alpha\beta}$. *I* is the nuclear spin of the quadrupolar nucleus.

H_Δ describes the torsional splitting between the $|0\rangle$ and $|1\rangle$ tunneling states

$$H_\Delta = \Delta E + \Delta E_J P^2 + \Delta E_K P_a^2 + \Delta E_2\left(P_+^2 + P^2_-\right) + \cdots \quad (8)$$

and H_c is the Coriolis operator which connects the two states

$$H_c = F_{ac}(P_aP_c + P_cP_a) + F_{bc}(P_bP_c + P_cP_b) + \cdots \quad (9)$$

The constants F_{ac} and F_{bc} as well as their higher order parameters are Coriolis coupling parameters; ΔE_J, ΔE_K, ΔE_2, and higher order parameters are centrifugal distortion parameters to ΔE which defines the difference between the *s* and *a* states [241–243].

In the microwave spectrum of dimethyl amine, ethyl methyl amine, and diethyl amine, the *s* and *a* states are separated by $\Delta E \approx$ 1323.0, 990.5, and 760.8 MHz, respectively. Consequently, all *c*-type transitions split into doublets separated by twice the value of ΔE, which is about 2646.0 MHz, 1981.0 MHz, and 1521.5 MHz, respectively. We recognize a trend that the larger the moclecule, the smaller the splittings. The Coriolis coupling operator H_c connects the *s* and *a* energy levels. According to selection rules, *b*-type transitions occur within a symmetry species. However, in the microwave spectrum recorded by high resolution molecular jet Fourier transform spectroscopy, narrow splittings of about 100 kHz could be observed due to Coriolis interaction in all molecules. These splittings are on the same order of magnitude as those of the fine splittings arising from the methyl internal rotations and are overlapped, making the assignments of *b*-type transitions in the microwave spectra of secondary amine quite challenging [232]. A typical spectrum of the $3_{12} \leftarrow 3_{03}$ *b*-type transition of ethyl methyl amine taken at a resolution of 2 kHz is given in Fig. 24. For comparison, Fig. 25 illustrates a spectrum of the $5_{15} \leftarrow 5_{05}$ *c*-type transition of the same molecule where the Coriolis tunneling splittings are not overlapped with the methyl torsional splittings. Because the inversion tunneling motion does not couple with the internal rotation of the two methyl groups, the latter effects can be neglected during the inversion tunneling treatment without affecting the fit quality, and treated separately to extract the torsional barrier height.

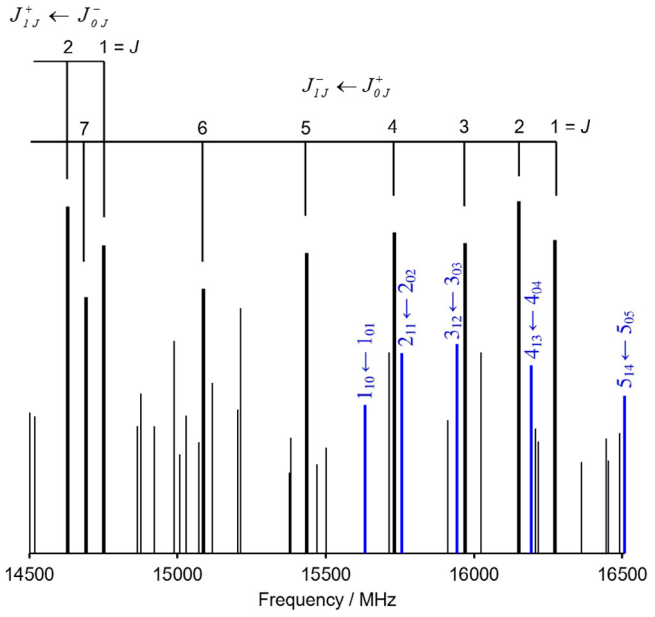

Fig. 23. The broadband scan in the range of 14500 to 16500 MHz of diethyl amine. Blue lines are *Q*-branch *b*-type transitions; thick lines indicate *c*-type transitions which split into doublets because of the proton tunneling.

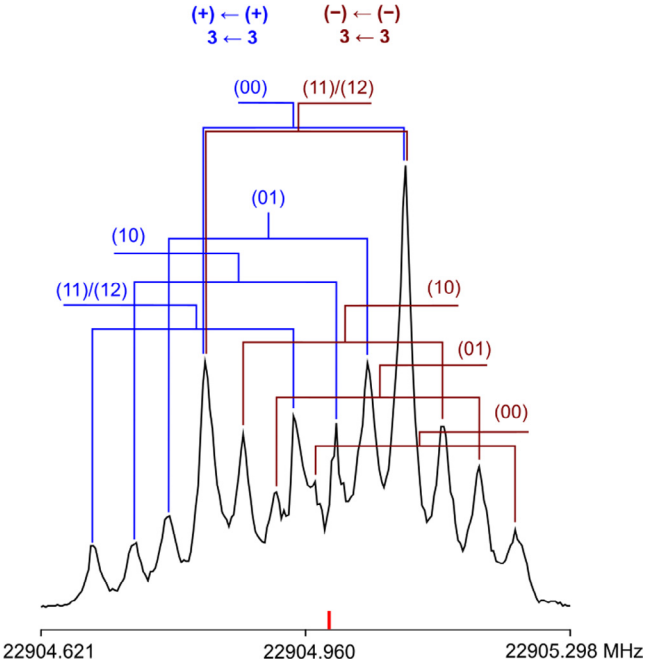

Fig. 24. The spectrum of the hyperfine component $F = 3 \leftarrow 3$ of the *b*-type $3_{12} \leftarrow 3_{03}$ transition of ethyl methyl amine measured at a polarization frequency of 22905.0 MHz (marked in red) [232]. All frequencies are given in MHz. The Doppler doublets are marked by brackets with the respective torsional species given in the notation introduced in Ref. 244. The corresponding $s \leftarrow s$ and $a \leftarrow a$ species are color-coded and given above each torsional block.

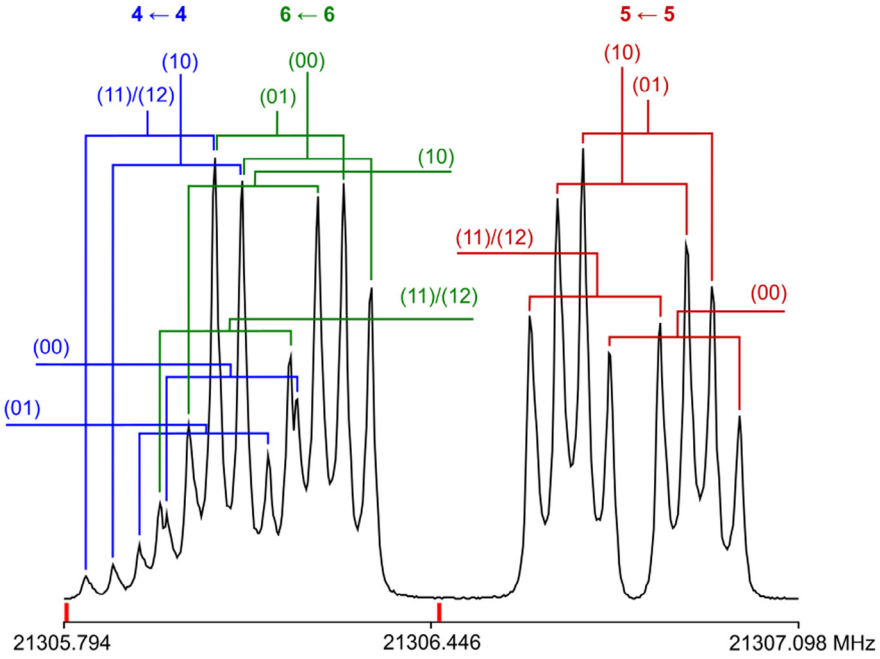

Fig. 25. The spectrum of the $a \leftarrow s$ component of the *c*-type transition $5_{15} \leftarrow 5_{05}$ of ethyl methyl amine [232]. Two spectra measured at the polarization frequencies of 21305.5 MHz and 21306.5 MHz (marked in red) are combined and the intensities are normalized. Brackets denote the Doppler splittings. The respective torsional species are given, and the ^{14}N quadrupole hyperfine component $F' \leftarrow F$ is above each torsional block.

6. Conclusion

Studying the structure and internal dynamics of a molecule relevant to topics as divers as astrophysics, molecular biology, environmental sciences, and atmospheric chemistry using high resolution spectroscopy has a long tradition and is still a lively research field with great potential. Many of those molecules experience large amplitude motions. The present review focuses on an extremely important type, inversion tunneling. Though not occuring as frequently as, for example, internal rotation, due to the frame symmetry required to obtain a symmetric double minimum potential, many molecules of great interest and importances feature this tunneling effect. The combination of high resolution spectroscopy, mainly in the microwave and infrared frequency ranges, group theoretical tunneling formalism, and theoretical studies is particularly successful in decoding spectra of molecules with inversion tunneling splittings and providing reference data for astrophysical research, atmospheric chemistry, or general applications in physical chemistry. The four molecules chosen to demonstrate the inversion tunneling effects are ammonia with its umbrella motion during which the nitrogen atom passes from one side of the plane formed by the three hydrogens to the other, methylamine with the inversion motion of the amino group coupled with a methyl internal rotation, hydrazine with complex internal dynamics governed by two amino tunneling motions and an internal rotation of the two amino groups around the N-N bond, and secondary amines with the inversion tunneling of the hydrogen atom attached to the nitrogen.

Declaration of Competing Interest

The authors declare that they have no known competing financial interests or personal relationships that could have appeared to influence the work reported in this paper.

Acknowledgements

This work was supported by the Agence Nationale de la Recherche ANR (project ID ANR-18-CE29-0011) and partly supported by the Programme National Physique et Chimie du Milieu Intestellaire (PCMI) of CNRS/INSU with INC/INP co-funded by CEA and CNES.

References

[1] A. Otte, Nature 580 (2020) 29.
[2] M. Kemp, Nature 394 (1998) 25.
[3] D. Schilter, Nat. Rev. Chem. 3 (2019) 511.
[4] W.M. Bloch, A. Burgun, C.J. Coghlan, R. Lee, et al., Nat. Chem. 6 (2014) 906.
[5] Y. Li, S. Tang, A. Yusov, J. Rose, et al., Nat. Commun. 10 (2019) 4477.
[6] M.J. Suggit, A. Higginbotham, J.A. Hawreliak, G. Mogni, et al., Nat. Commun. 3 (2012) 1224.
[7] M. Hess, T. Sasaki, C. Villevieille, P. Novák, Nat. Commun. 6 (2015) 8169.
[8] Y. Morinaka, S. Sato, A. Wakamiya, H. Nikawa, et al., Nat. Commun. 4 (2013) 1554.
[9] F. Meirer, B.M. Weckhuysen, Nat. Rev. Mater. 3 (2018) 324.
[10] F. Bertolotti, D.N. Dirin, M. Ibáñez, F. Krumeich, et al., Nat. Mater. 15 (2016) 987.
[11] Y. Inokuma, S. Yoshioka, J. Ariyoshi, T. Arai, et al., Nature 495 (2013) 461.
[12] J.M. Thomas, Nature 491 (2012) 186.
[13] J. Hughes, Nature 452 (2008) 30.
[14] Nobel Prize for Chemistry: Prof. P. Debye, Nature 138, 873 (1936).
[15] J. Watson, F. Crick, Nature 171 (1953) 737.
[16] M.F. Perutz, M.G. Rossmann, A.F. Cullis, H. Muirhead, et al., Nature 185 (1960) 422.
[17] K. Holmes, Nature 389 (1997) 340.
[18] S. Frantz, Nat. Rev. Mol. Cell. Biol. 3 (2002) 146.
[19] The 1964 Nobel Prize for Chemistry: Prof. Dorothy Crowfoot Hodgkin, F.R.S., Nature 204, 922 (1964).
[20] J. Howard, Nat. Rev. Mol. Cell. Biol. 4 (2003) 891.
[21] W. Gordy, R.L. Cook, Microwave Molecular Spectra, 3rd edition., John Wiley & Sons, New York, 1984.
[22] W. Caminati, J.-U. Grabow, J. Am. Chem. Soc. 128 (2006) 854.
[23] M. Schnell, J.-U. Grabow, Angew. Chem. Int. Ed. 45 (2006) 3465.
[24] J. Thomas, O. Sukhorukov, W. Jäger, Y. Xu, Angew. Chem. Int. Ed. 52 (2013) 4402.

[25] I. Uriarte, A. Insausti, E.J. Cocinero, A. Jabri, et al., J. Phys. Chem. Lett. 9 (2018) 5906.
[26] A. Lesarri, S.T. Shipman, J.L. Neill, G.G. Brown, et al., J. Am. Chem. Soc. 132 (2010) 13417.
[27] G.R. Gunther-Mohr, R.L. White, A.L. Schawlow, W.E. Good, D.K. Coles, Phys. Rev. 94 (1954) 1184.
[28] K.M. Marstokk, H. Møllendal, J. Mol. Struct. 49 (1978) 221.
[29] T. Kasuja, Sci. Papers Inst. Phys. Chem. Res. Tokyo 56 (1962) 1.
[30] L. Ferres, H. Mouhib, W. Stahl, M. Schwell, H.V.L. Nguyen, J. Mol. Spectrosc. 337 (2017) 59.
[31] S. Albert, P. Lerch, R. Prentner, M. Quack, Angew. Chem. Int. Ed. 52 (2013) 346.
[32] J.H. Baraban, M.-A. Martin-Drumel, P.B. Changala, S. Eibenberger, et al., Angew. Chem. Int. Ed. 57 (2018) 1821.
[33] M. Schnell, U. Erlekam, P.R. Bunker, G. von Helden, et al., Angew. Chem. Int. Ed. 52 (2013) 5180.
[34] W. Li, L. Evangelisti, Q. Gou, W. Caminati, R. Meyer, Angew. Chem. Int. Ed. 58 (2019) 859.
[35] G. Feng, Q. Gou, L. Evangelisti, W. Caminati, Angew. Chem. Int. Ed. 53 (2014) 530.
[36] S. Ghosh, J. Thomas, W. Huang, Y. Xu, W. Jäger, J. Phys. Chem. Lett. 6 (2015) 3126.
[37] B.M. Giuliano, W. Caminati, Angew. Chem. Int. Ed. 44 (2005) 603.
[38] M.E. Sanz, A. Lesarri, J.C. López, J.L. Alonso, Angew. Chem. Int. Ed. 40 (2001) 935.
[39] W. Caminati, Microwave Spectroscopy of Large Molecules and Molecular Complexes, Chapter in book: Handbook of High-resolution Spectroscopy, John Wiley & Sons Ltd, 2011.
[40] M.A. Duncan, Annu. Rev. Phys. Chem. 48 (1997) 69.
[41] K. Fuke, K. Hashimoto, S. Iwata, Adv. Chem. Phys. 110 (1999) 431.
[42] J.M. Farrar, Int. Rev. Phys. Chem. 22 (2003) 593.
[43] J.M. Lisy, Int. Rev. Phys. Chem. 16 (1997) 267.
[44] R.S. Walters, E.D. Pillai, M.A. Duncan, J. Am. Chem. Soc. 127 (2005) 16599.
[45] A.I. Boldyrev, O.P. Charkin, J. Struct. Chem. 26 (1985) 451.
[46] I. Omae, Chem. Rev. 79 (1979) 287.
[47] M. Ciampolini, G.P. Sparoni, Inorg. Chem. 5 (1966) 45.
[48] T.W. Swaddle, Can. J. Chem. 55 (1977) 3166.
[49] H.-F. Zhu, L.-Y. Kong, T. Okamura, J. Fan, W.-Y. Sun, N. Ueyama, Eur. J. Inorg. Chem. 1465 (2004).
[50] J.C. Thompson, Electrons in Liquid Ammonia, Oxford University Press, New York, 1976.
[51] T.E. Salter, A.M. Ellis, J. Chem. Phys. 127 (2007) 144314.
[52] F.S. Abyaneh, M.E. Moghadam, A. Divsalar, D. Ajloo, M.H. Sadr, Appl. Biochem. Biotechnol. 186 (2018) 271.
[53] S. Tsunekawa, T. Kojima, J.T. Hougen, J. Mol. Spectrosc. 95 (1982) 133.
[54] K.C. Patil, T.M. Rattan, Inorganic Hydrazine Derivatives, John Wiley & Sons, Ltd., 2014.
[55] S.L. Tey, M.V. Reddy, G.V.S. Rao, B.V.R. Chowdari, et al., Chem. Mater. 18 (2006) 1587.
[56] S.T. Aruna, K.C. Patil, J. Mater. Synth. Process. 4 (1996) 175.
[57] B.T. Heaton, C. Jacob, P. Page, Coord. Chem. Rev. 154 (1996) 193.
[58] P. Brandi-Blanco, P.J. Sanz Miguel, B. Lippert, Dalton Trans. 40 (2011) 10316.
[59] M.W. Davies, A.J. Clarke, G.J. Clarkson, M. Shipman, J.H. Tucker, Chem. Commun. 47 (2007) 5078.
[60] A. Tomić, B. Kovačević, S. Tomić, Phys. Chem. Chem. Phys. 18 (2016) 27245.
[61] I. Merke, L.H. Coudert, J. Mol. Spectrosc. 237 (2006) 174.
[62] M. Kręglewski, J. Mol. Spectrosc. 133 (1989) 10.
[63] B. Kleibömer, D.H. Sutter, Z. Naturforsch. 43a (1988) 561.
[64] T. Tsuji, H. Sekiya, Y. Nishimura, A. Mori, H. Takeshita, J. Chem. Phys. 95 (1991) 4802.
[65] R.L. Redington, T.E. Redington, R.L. Sams, J. Phys. Chem. A 112 (2008) 1480.
[66] H. Ozeki, M. Takahashi, K. Okuyama, K. Kimura, J. Chem. Phys. 99 (1993) 56.
[67] S. Takada, H. Nakamura, J. Chem. Phys. 102 (1995) 3977.
[68] H. Abe, N. Mikami, M. Ito, J. Phys. Chem. 86 (1982) 1768.
[69] Y. Tomioka, M. Ito, N. Mikami, J. Phys. Chem. 87 (1983) 4401.
[70] R.K. Frost, F.C. Hagemeister, C.A. Arrington, D. Schleppenbach, T.S. Zwier, K.D. Jordan, J. Chem. Phys. 105 (1996) 2605.
[71] A. Mitsuzuka, A. Fujii, T. Ebata, N. Mikamia, J. Chem. Phys. 105 (1996) 2618.
[72] T. Taniguchi, A. Tsubouchi, Y. Imai, J. Yuasa, H. Oguri, J. Org. Chem. 83 (2018) 15284.
[73] L. Clarisse, C. Clerbaux, F. Dentener, D. Hurtmans, P.F. Coheur, Nat. Geosci. 2 (2009) 479.
[74] M. Van Damme, L. Clarisse, S. Whitburn, J. Hadji-Lazaro, et al., Nature 564 (2018) 99.
[75] L.-M. Lara, B. Bézard, C.A. Griffith, J.H. Lacy, T. Owen, Icarus 131 (1998) 317.
[76] A. Burrows, M. Marley, W.B. Hubbard, J.I. Lunine, et al., Astrophys. J. 491 (1997) 856.
[77] C.M. Sharp, A. Burrows, Astrophys. J. 168 (2007) 140.
[78] J.-P. Beaulieu, G. Tinetti, D.M. Kipping, I. Ribas, et al., Astrophys. J. 731 (2011) 16.
[79] P.R. Bunker, P. Jensen, Molecular Symmetry and Spectroscopy, NRC Research Press, Ottawa, Ontario, Canada, 2006.
[80] I. Kleiner, G. Tarrago, L.R. Brown, J. Mol. Spectrosc. 173 (1995) 120.
[81] I. Kleiner, L.R. Brown, G. Tarrago, Q.-L. Kou, et al., J. Mol. Spectrosc. 193 (1999) 46.
[82] G. Geulachvili, A.H. Abdullah, N. Tu, K.N. Rao, et al., J. Mol. Spectrosc. 133 (1989) 345.
[83] C. Cottaz, I. Kleiner, G. Tarrago, L.R. Brown, et al., J. Mol. Spectrosc. 203 (2000) 285.
[84] C. Cottaz, G. Tarrago, I. Kleiner, L.R. Brown, J. Mol. Spectrosc. 209 (2001) 30.
[85] J.C. Pearson, S. Yu, O. Pirali, J. Chem. Phys. 145 (2016) 124301.
[86] M. Guinet, P. Jeseck, D. Mondelain, I. Pepin, et al., J. Quant. Spectrosc. Radiat. Transf. 112 (2011) 1950.
[87] M. Fabian, K. Yamada, J. Mol. Spectrosc. 198 (1999) 102.
[88] V. Nemtchinov, K. Sung, P. Varanasi, J. Quant. Spectrosc. Radiat. Transf. 83 (2004) 243.
[89] H. Aroui, S. Nouri, J. Bouanich, J. Mol. Spectrosc. 220 (2003) 248.
[90] Z. Chu, L. Chen, P.K. Cheo, J. Quant. Spectrosc. Radiat. Transf. 51 (1994) 591.
[91] L.S. Rothman, I.E. Gordon, A. Barbe, D.C. Benner, et al., J. Quant. Spectrosc. Radiat. Transf. 110 (2009) 533.
[92] M.J. Down, C. Hill, S.N. Yurchenko, J. Tennyson, et al., J. Quant. Spectrosc. Radiat. Transf. 130 (2013) 260.
[93] V. Spirko, J.M.R. Stone, D. Papoušek, J. Mol. Spectrosc. 60 (1976) 159.
[94] S. Urban, J. Mol. Spectrosc. 131 (1988) 133.
[95] P. Pracna, V. Spirko, W.P. Kraemer, J. Mol. Spectrosc. 136 (1989) 317.
[96] D. Papoušek, J.M.R. Stone, V. Spirko, J. Mol. Spectrosc. 48 (1973) 17.
[97] W.S. Benedict, E.D. Plyler, E.D. Tidwell, J. Chem. Phys. 29 (1958) 829.
[98] L.R. Brown, J.S. Margolis, J. Quant. Spectrosc. Radiat. Transf. 56 (1996) 283.
[99] P. Cacciani, P. Čermák, J. Cosléou, J. El Romh, et al., Mol. Phys. 112 (2014) 2476.
[100] X. Huang, D.W. Schwenke, T.J. Lee, J. Chem. Phys. 129 (2008) 214304.
[101] S.N. Yurchenko, R.J. Barber, A. Yachmenev, W. Thiel, et al., J. Phys. Chem. A 113 (2009) 11845.
[102] S.N. Yurchenko, R.J. Barber, J. Tennyson, Mon. Not. R. Astr. Soc. 413 (2011) 1828.
[103] S.N. Yurchenko, R.J. Barber, J. Tennyson, W. Thiel, P. Jensen, J. Mol. Spectrosc. 268 (2011) 123.
[104] S.N. Yurchenko, J. Zheng, H. Lin, P. Jensen, W. Thiel, J. Chem. Phys. 123 (2005) 134308.
[105] S.N. Yurchenko, W. Thiel, P. Jensen, J. Mol. Spectrosc. 245 (2007) 126.
[106] A.E. Lynas-Gray, S. Miller, J. Tennyson, J. Mol. Spectrosc. 169 (1995) 458.
[107] L. Lodi, J. Tennyson, O.L. Polyansky, J. Chem. Phys. 135 (2011) 034113.
[108] P. Herbine, T.R. Dyke, J. Chem. Phys. 83 (1985) 3768.
[109] P.A. Stockman, R.E. Bumgarner, S. Suzuki, G.A. Blake, J. Chem. Phys. 96 (1992) 2496.
[110] Z. Latajka, S. Scheiner, J. Phys. Chem. 94 (1990) 217.
[111] D.A. Rodham, S. Suzuki, R.D. Suenram, F.J. Lovas, et al., Nature 632 (1993) 735.
[112] G.T. Fraser, K.R. Leopold, W. Klemperer, J. Chem. Phys. 80 (1984) 1423.
[113] G.T. Fraser, F.J. Lovas, R.D. Suenram, D.D. Nelson Jr., W. Klemperer, J. Chem. Phys. 84 (1986) 5983.
[114] D.D. Nelson, G.T. Fraser, K.I. Peterson, K. Zhao, W. Klemperer, J. Chem. Phys. 85 (1986) 5512.
[115] G.T. Fraser, R.D. Suenram, F.J. Lovas, W.J. Stevens, Chem. Phys. 12 (1988) 31.
[116] L.A. Surin, I.V. Tarabukin, S. Schlemmer, A.A. Breier, et al., Astrophys. J. 838 (2017) 272017.
[117] M.D. Albaqami, A.M. Ellis, Chem. Phys. Lett. 706 (2018) 736.
[118] K. Ohashi, K. Inoue, T. Iino, J. Sasaki, et al., J. Mol. Liq. 147 (2009) 71.
[119] K. Inoue, K. Ohashi, T. Iino, J. Sasaki, et al., Phys. Chem. Chem. Phys. 10 (2008) 3052.
[120] T. Imamura, K. Ohashi, J. Sasaki, K. Inoue, et al., Phys. Chem. Chem. Phys. 12 (2010) 11647.
[121] J. Kozubal, T.R. Heck, R.B. Metz, J. Phys. Chem. A 123 (2019) 4929.
[122] P.D. Holtom, C.J. Bennett, Y. Osamura, N.J. Mason, R.I. Kaiser, Astrophys. J. 626 (2005) 940.
[123] J.B. Bossa, F. Duvernay, P. Theulé, et al., Astronom. Astrophys. 506 (2009) 601.
[124] C.W. Lee, J.K. Kim, E.S. Moon, Y.C. Minth, H. Kang, Astrophys. J. 697 (2009) 428.
[125] P. Ehrenfreund, M.P. Bernstein, J.P. Dworkin, S.A. Sandford, L.J. Allamandola, Astrophys. J. 550 (2001) L95.
[126] N. Fourikis, K. Takagi, M. Morimoto, Astrophys. J. 191 (1974) L139.
[127] N. Kaifu, M. Morimoto, K. Nagane, K. Akabane, et al., Astrophys. J. 191 (1974) L135.
[128] S. Muller, A. Beelen, M. Guelin, S. Aalto, et al., Astronom. Astrophys. 535 (2011) A103.
[129] D.P. Glavin, J.P. Dworkin, S.A. Sandford, Met. Planet. Sci. 43 (2008) 399.
[130] E.G. Bogelund, A.B. McGuire, M.R. Hogerheijde, E.F. Dishoeck, N.F.W. Ligterink, Astronom. Astrophys. 624 (2019) A82.
[131] B. Podolsky, Phys. Rev. 32 (1928) 812.
[132] M. Kręglewski, in: Structures and Conformations of Non-Rigid Molecules, Kluwer Academic Publishers, 1993, pp. 29–43.
[133] N. Ohashi, J.T. Hougen, J. Mol. Spectrosc. 121 (1987) 474.
[134] H.C. Longuet-Higgins, Mol. Phys. 6 (1963) 445.
[135] H.W. Kroto, Molecular Rotation Spectra, John Wiley & Sons, London, 1975.
[136] D. Papoušek, J.M.R. Stone, V. Špirko, J. Mol. Spectrosc. 48 (1973) 17.
[137] M. Tsuboi, A.Y. Hirakawa, K. Tamagake, J. Mol. Spectrosc. 22 (1967) 272.
[138] K. Takagi, T. Kojima, J. Phys. Soc. Lpn. 30 (1971) 1145.
[139] C. Belorgeot, V. Stern, N. Goff, K. Kachamrsky, K.D. Möller, J. Mol. Spectrosc. 92 (1982) 91.
[140] T. Ijima, Bull. Chem. Soc. Jpn. 59 (1986) 853.
[141] M. Oda, N. Ohashi, J.T. Hougen, J. Mol. Spectrosc. 142 (1990) 57.
[142] J.R. Durig, C. Zheng, Struct. Chem. 12 (2001) 137.
[143] D.R. Lide Jr., J. Chem. Phys. 22 (1954) 1613.
[144] K. Shimoda, T. Nishikawa, T. Itoh, J. Phys. Soc. Jpn. 9 (1954) 974.

[145] H. Hirakawa, A. Miyahara, K. Shimoda, J. Phys. Soc. Jpn. 11 (1956) 334.
[146] T. Nishikawa, J. Phys. Soc. Jpn. 12 (1957) 668.
[147] K. Takagi, T. Kojima, Astrophys. J. 181 (1973) L91.
[148] N. Ohashi, K. Takagi, J.T. Hougen, W.B. Olson, W.J. Lafferty, J. Mol. Spectrosc. 126 (1987) 443.
[149] M. Kręglewski, G. Wlodarczak, J. Mol. Spectrosc. 156 (1992) 383.
[150] V.V. Ilyushin, E.A. Alekseev, S.F. Dyubko, R.A. Motiyenko, J.T. Hougen, J. Mol. Spectrosc. 229 (2005) 170.
[151] M. Kręglewski, W. Stahl, J.-U. Grabow, G. Wlodarczak, Chem. Phys. Lett. 196 (1992) 155.
[152] V. Ilyushin, F.J. Lovas, J. Phys. Chem. Ref. Data 36 (2007) 1141.
[153] R.A. Motiyenko, V.V. Ilyushin, B.J. Drouin, S. Yu, L. Margulès, Astronom. Astrophys. 563 (2014) A137.
[154] N. Ohashi, K. Takagi, J.T. Hougen, W.B. Olson, W.L. Lafferty, J. Mol. Spectrosc. 132 (1988) 242.
[155] N. Ohashi, S. Tsunekawa, K. Takagi, J.T. Hougen, J. Mol. Spectrosc. 137 (1989) 33.
[156] I. Gulaczyk, M. Kręglewski, V.-M. Horneman, J. Mol. Spectrosc. 342 (2017) 25.
[157] M. Oda, N. Ohashi, J. Mol. Spectrosc. 138 (1989) 246.
[158] N. Ohashi, H. Shimada, W.B. Olson, K. Kawaguchi, J. Mol. Spectrosc. 152 (1992) 298.
[159] I. Gulaczyk, M. Kręglewski, V.-M. Horneman, J. Quant. Spectrosc. Radiat. Transf. 217 (2018) 321.
[160] I. Gulaczyk, M. Kręglewski, J. Quant. Spectrosc. Radiat. Transf. 252 (2020) 107097.
[161] I. Kleiner, J.T. Hougen, J. Phys. Chem. A 119 (2015) 10664.
[162] I. Kleiner, J.T. Hougen, J. Mol. Spectrosc. 368 (2020) 111255.
[163] M. Kręglewski, F. Winther, J. Mol. spectrosc. 156 (1992) 261.
[164] L. Sztraka, S. Alanko, M. Koivusaari, J. Mol. Struct. 410–411 (1997) 391.
[165] I. Gulaczyk, W. Łodyga, M. Kręglewski, V.-M. Horneman, Mol. Phys. 108 (2010) 2389.
[166] I. Gulaczyk, M. Kręglewski, J. Mol. Spectrosc. 256 (2009) 86.
[167] I. Gulaczyk, M. Kręglewski, V.-M. Horneman, J. Mol. Spectrosc. 270 (2011) 70.
[168] R.M. Lees, Z.-D. Sun, B.E. Billinghurst, J. Chem. Phys. 135 (2011) 104306.
[169] S.F. Dyubko, V.A. Svich, L.D. Fesenko, J. Exp. Theor. Phys. Lett. 16 (1972) 418.
[170] T.K. Plant, P.B. Coleman, T.A. de Temple, IEEE J. Quantum Electron. QE-9 (1973) 962.
[171] R.M. Lees, Z.-D. Sun, L.-H. Xu, Int. J. Infrared Milli Waves 29 (2008) 148.
[172] Z.-D. Sun, S.-D. Qi, R.M. Lee, L.-H. Xu, Sci. Rep. 6 (2016) 34270.
[173] M.B. Dawadi, C.M. Lindsay, A. Chirokolava, D.S. Perry, L.-H. Xu, J. Chem. Phys. 138 (2013) 104305.
[174] M.B. Dawadi, R.S. Bhatta, D.S. Perry, J. Phys. Chem. A 117 (2013) 13356.
[175] I. Gulaczyk, M. Kręglewski, P. Asselin, O. Pirali, I. Kleiner, Can. J. Phys. 98 (2020) 560.
[176] S.J. Lee, B.J. Mhin, S.J. Cho, J.Y. Lee, K.S. Kim, J. Phys. Chem. 98 (1994) 1129.
[177] G.I. Csonka, L. Sztraka, Chem. Phys. Lett. 233 (2000) 611.
[178] Y.G. Smeyers, M. Villa, Chem. Phys. Lett. 324 (2000) 273.
[179] M. Pelegrini, O. Roberto-Neto, F.B.C. Machado, Chem. Phys. Lett. 414 (2005) 495.
[180] C. Levi, J.M.L. Martin, I. Bar, J. Comput. Chem. 29 (2008) 1268.
[181] H.-W. Kim, D. Zeroka, Int. J. Quantum Chem. 108 (2008) 974.
[182] L.C. Ducati, R. Custodito, R. Rittner, Int. J. Quantum Chem. 110 (2010) 2006.
[183] Y.G. Smeyers, M. Villa, M.L. Senent, J. Mol. Spectrosc. 177 (1996) 66.
[184] Y.G. Smeyers, M. Villa, M.L. Senent, J. Mol. Spectrosc. 191 (1998) 232.
[185] M. Kreglewski, J. Mol. Spectrosc. 72 (1978) 1.
[186] M.L. Senent, J. Mol. Spectrosc. 343 (2018) 28.
[187] A.G. Baca, M.A. Schulz, D.A. Shirley, J. Chem. Phys. 83 (1985) 6001.
[188] T.S. Nunney, J.J. Birtill, R. Raval, Surf. Sci. 427–428 (1999) 282–287.
[189] W. Erley, J.C. Hemminger, Surf. Sci. 316 (1994) L1025.
[190] D. Jentz, M. Trenary, X.D. Peng, P. Stair, Surf. Sci. 341 (1995) 282.
[191] D. Bogachuk, L. Wagner, S. Mastroianni, M. Daub, et al., J. Mater. Chem. A 8 (2020) 9788.
[192] A. Cruz-Navarro, D. Hernández-Romero, A. Flores-Parra, J.M. Rivera, et al., Coord. Chem. Rev. 427 (2021) 213587.
[193] T. Kasuya, T. Kojima, J. Phys. Sec. Japan 18 (1963) 364.
[194] D. Papoušek, K. Sarka, V. Špirko, B. Jordanov, Collect. Czech. Chem. Commun. 36 (1971) 890.
[195] A.J. Merer, J.K.G. Watson, J. Mol. Spectrosc. 47 (1973) 499.
[196] J.T. Hougen, J. Mol. Spectrosc. 89 (1981) 296.
[197] N. Ohashi, J.T. Hougen, J. Mol. Spectrosc. 112 (1985) 384.
[198] P.A. Giguere, I.D. Liu, J. Chem. Phys. 20 (1952) 136.
[199] S. Tsunekawa, T. Kojima, J.T. Hougen, J. Mol. Spectrosc. 95 (1982) 133–152.
[200] N. Ohashi, W.J. Lafferty, W.B. Olson, J. Mol. Spectrosc. 117 (1986) 119.
[201] A. Yamaguchi, I. Ichishima, T. Simanouchi, S. Mizushima, Spectrochim. Acta 16 (1960) 1471.
[202] N. Ohashi, W.B. Olson, J. Mol. Spectrosc. 145 (1991) 383.
[203] Y. Hamada, A.Y. Hirakawa, K. Tamagake, M. Tsuboi, J. Mol. Spectrosc. 35 (1970) 420.
[204] M. Tsuboi, J. Overend, J. Mol. Spectrosc. 52 (1974) 256.
[205] H. Jones, M. Takami, J. Chem. Phys. 78 (1983) 1039.
[206] M. Tsuboi, Y. Hamada, L. Henry, J. Chazelas, A. Valentin, J. Mol. Spectrosc. 108 (1984) 328.
[207] N. Ohashi, L. Henry, J. Chazelas, A. Valentin, J. Mol. Spectrosc. 161 (1993) 560.
[208] I. Gulaczyk, M. Kręglewski, A. Valentin, J. Mol. Spectrosc. 186 (1997) 246.
[209] N. Ohashi, M. Masue, J. Mol. Spectrosc. 150 (1991) 238.
[210] I. Gulaczyk, M. Kręglewski, J. Mol. Spectrosc. 249 (2008) 73.
[211] I. Gulaczyk, J. Pyka, M. Kręglewski, J. Mol. Spectrosc. 241 (2007) 75.
[212] I. Gulaczyk, M. Kręglewski, A. Valentin, J. Mol. Spectrosc. 220 (2003) 132.
[213] W. Łodyga, M. Kręglewski, Chem. Phys. Lett. 210 (1993) 303.
[214] W. Łodyga, M. Kręglewski, J. Makarewicz, J. Mol. Spectrosc. 183 (1997) 374.
[215] W. Łodyga, J. Makarewicz, J. Chem. Phys. 136 (2012) 174301.
[216] A.T. Kowal, J. Mol. Struct. 625 (2003) 71.
[217] N.J. Wright, R.B. Gerber, J. Chem. Phys. 114 (2001) 8763.
[218] F.B.C. Machado, O. Roberto-Neto, Chem. Phys. Lett. 352 (2002) 120.
[219] J.R. Durig, C. Zheng, Vib. Spectrosc. 30 (2002) 59.
[220] M.F. Iskander, L. El Sayed, M.A. Lasheen, Inorg. Chim. Acta 16 (1976) 147.
[221] L. El, M.F. Iskander Sayed, J. Inorg. Nucl. Chem. 33 (1971) 435.
[222] L. Sacconi, A. Sabatini, J. Inorg. Nucl. Chem. 25 (1963) 1389.
[223] D. Nicolls, R. Swindells, J. Inorg. Nucl. Chem. 30 (1968) 2211.
[224] R.C. Aggarwal, K.K. Narang, Inorg. Chim. Acta 74 (1973) 651.
[225] T. Sandmeier, F.W. Goetzke, S. Krautwald, E.M. Carreira, J. Am. Chem. Soc. 141 (2019) 12212.
[226] R. Knitsch, D. Han, F. Anke, L. Ibing, H. Jiao, M.R. Hansen, Organometallics 38 (2019) 2714.
[227] A.D. Sutton, A.K. Burrell, D.A. Dixon, E.B. Garner III, et al., Science 331 (2011) 1426.
[228] U.B. Gawas, S.C. Mojumdar, V.M.S. Verenkar, J. Therm. Anal. Calorim. 100 (2010) 867.
[229] T. Mimani, P. Ravindranthan, K.C. Patil, Proc. Indian Acad. Sci., Chem. Sci. 99 (1987) 209.
[230] J.E. Wollrab, V.W. Laurie, J. Chem. Phys. 48 (1968) 5058.
[231] R.E. Penn, J.E. Boggs, J. Mol. Spectrosc. 47 (1973) 340.
[232] K.J. Koziol, W. Stahl, H.V.L. Nguyen, J. Chem. Phys. 153 (2020) 184308.
[233] H.V.L. Nguyen, W. Stahl, J. Chem. Phys. 135 (2011) 024310.
[234] A. Weber, Academic Press, Inc., 1st edition, 2 (1992).
[235] M. Riese, F. Ploeger, A. Rap, B. Vogel, et al., J. Geophys. 117 (2012) D16305.
[236] T. Blumestock, Atmos. Chem. Phys. 6 (2006) 897.
[237] D.O. Muhleman, R.T. Clancy, Appl. Opt. 34 (1995) 6067.
[238] B. Tercero, I. Kleiner, J. Cernicharo, H.V.L. Nguyen, et al., Astrophys. J. Lett. 770 (2013) L13.
[239] C.P. Endres, S. Schlemmer, P. Schilke, J. Stutzki, et al., J. Mol. Spectrosc. 327 (2016) 95.
[240] I. Kleiner, ACS Earth Space Chem. 3 (2019) 1812.
[241] D. Christen, H.S.P. Müller, Phys. Chem. Chem. Phys. 5 (2003) 3600.
[242] H.S.P. Müller, D. Christen, J. Mol. Spectrosc. 228 (2004) 298.
[243] B.J. Drouin, J. Mol. Spectrosc. 340 (2017) 1.
[244] L. Ferres, J. Cheung, W. Stahl, H.V.L. Nguyen, J. Phys. Chem. A 123 (2019) 3497.